

University of Nevada, Reno

**Study of Plasmon Resonances in Single Photoionization of Carbon
Fullerene Molecular Ions**

A thesis submitted in partial fulfillment of the
requirements for the degree of Master of Science in
Physics

by

Christopher M. Thomas

Dr. Ronald A. Phaneuf/Thesis Advisor

August, 2011



THE GRADUATE SCHOOL

We recommend that the thesis
prepared under our supervision by

CHRISTOPHER THOMAS

entitled

**Study Of Plasmon Resonances In Single Photoionization Of Carbon Fullerene
Molecular Ions**

be accepted in partial fulfillment of the
requirements for the degree of

MASTER OF SCIENCE

Ronald A. Phaneuf, Ph. D., Advisor

Peter Winkler, Ph. D., Committee Member

Christopher Herald, Ph. D., Graduate School Representative

Marsha H. Read, Ph. D., Dean, Graduate School

August, 2011

Abstract

Beams of carbon fullerene ions containing 40 to 84 carbon atoms were irradiated by monochromatized synchrotron radiation at photon energies ranging from 18-70 eV at 0.5 eV intervals. Single photoionization was studied over this energy range using a merged-beams research endstation at the Advanced Light Source and absolute photoionization cross sections were measured. Electric-dipole-excited surface and volume plasmon resonances due to collective excitations of valence electrons were characterized and quantified by Lorentzian fits. Resonance parameters such as lifetimes and oscillator strengths were calculated and compared. Results for the photoionization of C_{60}^+ were compared to previously reported measurements. At higher photon energies, single photoionization accompanied by fragmentation of carbon pairs becomes relatively more important compared to pure single ionization and needs to be considered.

Acknowledgements

Many people have helped me en route to the completion of this thesis and I would like to thank them. First, and foremost, I would like to thank my outstanding advisor Dr. Ronald Phaneuf. Without his guidance and patience, I would not have been able to gain the knowledge and experience needed to be a great experimental physicist. He challenged me to work outside of my comfort zone, but still provided assistance when needed. My fellow students, Kiran Baral, Nagendra Aryal, and David Esteves provided me with great help while working at the ALS. They were willing to show me things over and over again until I fully understood them and their assistance with data analysis gave me confidence in my results. The beamline scientists I worked closely with, Dr. Alex Aguilar and Dr. David Kilcoyne provided me with great insight on how the beamline worked, which gave me a very good idea of how to diagnose and begin to resolve issues when they arose. Both provided support that made the experiments at the ALS successful.

I would also like to express my thanks to my committee members, Dr. Peter Winkler and Dr. Chris Herald. I did take classes from both of these professors and they gave me challenges that helped me become a better problem solver. I would like to express my gratitude to the professors in the physics department that helped me grow as a scientist through their knowledge expressed in the classroom. Dr. Aaron Covington has been a mentor of mine since I was an undergraduate. He provided me with challenges

when I worked on my senior thesis and always gave me a few minutes when I needed some advice. Without him, I do not where I would be.

I would like to thank my friends and family, especially my parents Barbara and Gary Hepworth, for their love and support throughout my life. They have always made me push and challenge myself, to become a better person. Last, and most importantly, I would like to thank my beloved wife Lysa for her continued support and love as I continue my college career.

Table of Contents

Abstract	i
Acknowledgements	ii
Table of Contents	iv
List of Tables	vi
List of Figures	ix
1 Introduction	1
1.1 Brief History of Fullerene Research.....	1
1.2 Motivations.....	4
2 Theoretical Background	5
2.1 Introduction.....	5
2.2 Photoionization.....	5
2.3 Giant Resonances.....	7
2.4 Geometry of Fullerenes.....	13
3 Experimental Set-up and Techniques	15
3.1 Introduction.....	15
3.2 Photon Beam.....	16
3.3 Ion Beam.....	18
3.4 Data Collection and Absolute Cross-Section Measurements.....	19
3.5 Higher-Order Radiation Correction.....	22

4 Photoionization of Carbon Fullerene Ions	24
4.1 Introduction.....	24
4.2 Photoionization of C_{40}^+	25
4.3 Photoionization of C_{50}^+	30
4.4 Photoionization of C_{70}^+	32
4.5 Photoionization of C_{76}^+	35
4.6 Photoionization of C_{78}^+	38
4.7 Photoionization of C_{84}^+	41
4.8 Photoionization of C_{60}^+	43
4.8.1 Present Measurements	44
4.8.2 Comparison with Published Data.....	46
4.9 Fullerene Comparisons.....	50
5 Summary, Conclusions, and Future Work	57
5.1 Summary and Conclusions.....	57
5.2 Future Work.....	60
References	62
Appendix: Tables of Absolute Photoionization Cross-Section Measurements	66

List of Tables

4.1 Parameters for C_{40}^+ Fits.....	28
4.2 Lorentzian Amplitude A and Oscillator Strengths for Surface and Volume Plasmons for C_{40}^+	29
4.3 Lifetimes of Plasmons for C_{40}^+	29
4.4 Plasmon Frequency Comparisons for C_{40}^+	29
4.5 Parameters for C_{50}^+ Fits.....	31
4.6 Lorentzian Amplitude A and Oscillator Strengths for Surface and Volume Plasmons for C_{50}^+	32
4.7 Lifetimes of Plasmons for C_{50}^+	32
4.8 Frequency Comparisons for C_{50}^+	32
4.9 Parameters for C_{70}^+ Fits.....	34
4.10 Lorentzian Amplitude A and Oscillator Strengths for Surface and Volume Plasmons for C_{70}^+	35
4.11 Lifetimes of Plasmons for C_{70}^+	35
4.12 Frequency Comparisons for C_{70}^+	35
4.13 Parameters for C_{76}^+ Fits.....	36

4.14 Lorentzian Amplitude A and Oscillator Strengths for Surface and Volume Plasmons for C_{76}^+	37
4.15 Lifetimes of Plasmons for C_{76}^+	37
4.16 Frequency Comparisons for C_{76}^+	38
4.17 Parameters for C_{78}^+ Fits.....	39
4.18 Lorentzian Amplitude A and Oscillator Strengths for Surface and Volume Plasmons for C_{78}^+	40
4.19 Lifetimes of Plasmons for C_{78}^+	40
4.20 Frequency Comparisons for C_{78}^+	41
4.21 Parameters for C_{84}^+ Fits.....	43
4.22 Lorentzian Amplitude A and Oscillator Strengths for Surface and Volume Plasmons for C_{84}^+	43
4.23 Lifetimes of Plasmons for C_{84}^+	43
4.24 Frequency Comparisons for C_{84}^+	43
4.25 Parameters for C_{60}^+ Fits.....	45
4.26 Lorentzian Amplitude A and Oscillator Strengths for Surface and Volume Plasmons for C_{60}^+	46

4.27 Lifetimes of Plasmons for C_{60}^+	46
4.28 Frequency Comparisons for C_{60}^+	46
4.29 Comparisons of Energy, FWHM, and Oscillator Strengths Reported by Scully <i>et al.</i> and Those Presented in this Thesis.....	47
4.30 Comparison of Volume-to-Surface-Plasmon-Frequencies Ratios for All Fullerenes Reported in This Thesis.....	50
A.1 Absolute Photoionization Cross-Section Measurements for C_{40}^+	66
A.2 Absolute Photoionization Cross-Section Measurements for C_{50}^+	66
A.3 Absolute Photoionization Cross-Section Measurements for C_{60}^+	66
A.4 Absolute Photoionization Cross-Section Measurements for C_{70}^+	66
A.5 Absolute Photoionization Cross-Section Measurements for C_{76}^+	66
A.6 Absolute Photoionization Cross-Section Measurements for C_{78}^+	67
A.7 Absolute Photoionization Cross-Section Measurements for C_{84}^+	67

List of Figures

1.1 C ₆₀ molecule.....	1
1.2 Photoionization cross-section measurement of C ₆₀ ⁺ . Lorentz fits were used to display the two plasmons.....	3
2.1 Generic photoionization cross section of an atom or atomic ion.....	7
2.2 Comparison of giant resonances in C nucleus, Xe atom, and C ₆₀	8
2.3 Isomers 30 and 32 of C ₉₀	14
2.4 Isomers of C ₆₈ and C ₇₂	14
3.1 Schematic of ECR ion source on IPB endstation.....	16
3.2 Schematic of beamline 10.0.1 optics.....	17
3.3 Schematic of ECR ion source on IPB endstation.....	19
3.4 Top Left, Right, and Bottom Left: Two-dimensional intensity profiles of the photon beam (solid) and ion beam (dashed). Bottom Right: Polynomial fit of measured form factors to estimate $F(z)$	22
3.5 Cross-section correction curves for higher-order radiation.....	23
4.1 Absolute cross-section measurement for single photoionization of C ₄₀ ⁺	26
4.2 Fits of plasmons (Lorentzians) and direct ionization background (linear) to the absolute cross-section measurement of C ₄₀ ⁺	27

4.3 Absolute cross-section measurement for the single photoionization of C_{50}^+	30
4.4 Fits of plasmons and direct ionization background for the absolute cross-section measurement of C_{50}^+	31
4.5 C_{70} molecule with carbon numbering	33
4.6 Absolute cross-section measurement for the single photoionization of C_{70}^+	33
4.7 Fits of plasmons and direct ionization background for the absolute cross-section measurement of C_{70}^+	34
4.8 Absolute cross-section measurement for the single photoionization of C_{76}^+	36
4.9 Fits of plasmons and direct ionization background for the absolute cross-section measurement of C_{76}^+	37
4.10 Absolute cross-section measurement for the single photoionization of C_{78}^+	39
4.11 Fits of plasmons and direct ionization background for the absolute cross-section measurement of C_{78}^+	40
4.12 Absolute cross-section measurement for the single photoionization of C_{84}^+	41
4.13 Fits of plasmons and direct ionization background for the absolute cross-section measurement of C_{84}^+	42
4.14 Absolute cross-section measurement for the single photoionization of C_{60}^+	44
4.15 Fits of plasmons and direct ionization background for the absolute cross-section measurement of C_{60}^+	45
4.16 Comparison of single photoionization and single photoionization + fragmentation of C_{60}^+	48
4.17 Comparison of the photon flux recorded by calibrated photodiodes of different types used in experiments on the IPB endstation	49

4.18 Comparison of surface and volume plasmon peak energy positions for the different fullerene molecular ions.....	51
4.19 Comparison of surface and volume plasmon widths for the different fullerene molecular ions.....	52
4.20 Comparison of surface and volume plasmon oscillator strengths for the different fullerene molecular ions.....	53
4.21 Comparison of plasmon lifetimes.....	54
4.22 Comparison of oscillations each plasmon experiences before decaying.....	55
5.1 Quasi-One-Dimensional Fragmentation Scan of C_{70}^+ at Photon Energies of 22, 35, and 65 eV.....	59
5.2 Two-dimensional photoionization/fragmentation scan of C_{70}^+ at 22eV.....	60
5.3 Excess Xe 4d cross section for double ionization with fragmentation of $Xe@C_{60}^+$	61

Chapter 1

Introduction

1.1 Brief History of Fullerene Research

The history of fullerenes spans across 25 years of research. The most stable of them, carbon-60 (C_{60}) was first discovered by Harold Kroto and collaborators at Rice University in 1985 [1] during laboratory experiments designed to understand carbon chain formation in interstellar space. A representation of C_{60} is shown in figure 1.1.

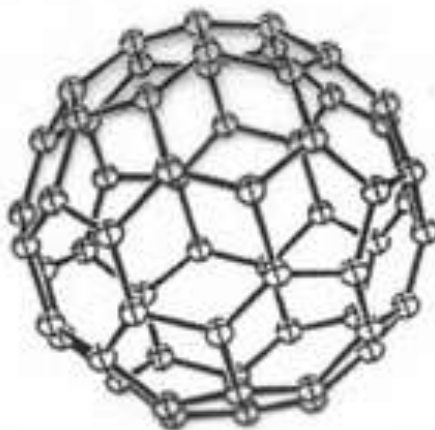


Figure 1.1 C_{60} molecule [2]

Using a Nd:YAG laser, carbon molecules were freed from the surface of a solid disk of graphite into a high-density helium flow. The carbon molecules were collimated into a molecular beam, photoionized by a separate laser, and detected by a time-of-flight mass spectrometer. On separate experiments, using different techniques and conditions, a

distinctive peak at mass 720 atomic mass units (amu), where an amu is 1/12 of the mass of a C atom, was observed. Harold Kroto, Robert Curl, and Richard Smalley won the 1996 Nobel Prize in Chemistry for their discovery.

Kroto believed that fullerenes could be distributed throughout the universe, due to their stability in violent environments, and that there is evidence that they could encage an atom or molecule, creating an endohedral fullerene. After studying Permian-Triassic Boundary sediments at sites in different parts of the world, Luann Becker and colleagues reported evidence of different fullerenes, ranging from C_{60} to C_{200} , existing in this layer [3]. Not only that, they also found noble gases trapped inside these fullerenes. Upon analysis, they found that the ratio of different noble gas isotopes, such as $^3\text{He}/^{36}\text{Ar}$, were not the same as the ratio on Earth, indicating that these endohedral fullerenes were delivered via an asteroid or comet collision on the Earth's surface. Another piece of evidence that these are of extraterrestrial origin is that in order for these fullerenes to form, a low-pressure hydrogen/high-pressure helium environment is needed [1, 3, 4]. Only stars or collapsing gas clouds are believed to provide the helium pressures needed to form fullerenes naturally.

It has been shown that neutral C_{60} and C_{70} both have a giant resonance near 20 eV in their photoabsorption spectrum that is described as a collective motion of the 240/280 valence electrons that surround the C_{60}/C_{70} cage. This so-called surface plasmon resonance was first reported by Hertel *et al.* [5] while studying photoionization of free C_{60} and C_{70} molecules. When looking at the photoionization spectrum for different charge states of the C_{60} ion, a second resonance was seen near 40 eV, a volume plasmon, by Scully *et al.* [6] at the Advanced Light Source (ALS) at Lawrence Berkeley National

Lab (LBNL). These high energy plasmon oscillations in fullerenes may result from electric dipole excitation, as confirmed by time-dependent density functional calculations. Figure 1.2 shows the cross-section measurement reported by Scully *et al.* [6] for $C_{60}^+ + h\nu \rightarrow C_{60}^{2+} + e^-$.

These high energy plasmon oscillations are the main focus of this thesis.

Experiments were conducted at the ALS beamline 10.0.1 Ion-Photon Beam (IPB) endstation. Varying the number of carbon atoms in the fullerene molecule, analysis of the plasmon energy positions and widths was conducted and is reported in chapter 4. Figure 1.2 shows the photoionization cross section for the single ionization of C_{60}^+ , as reported by Scully *et al.*

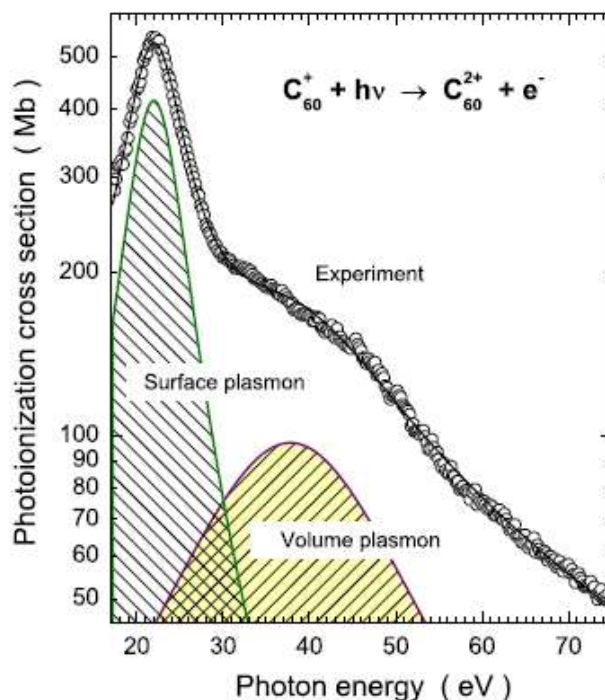


Figure 1.2 Photoionization cross-section measurement of C_{60}^+ [6]. Lorentz fits were used to display the two plasmons.

1.2 Motivations

The plasmons are interesting to study in the ionization spectrum of different fullerenes. They give insight into the photoionization mechanism and help to bridge the gap between a free molecule and a solid [6]. Aside from studying the plasmons, knowing the physics of how fullerenes act in different environments can help pave the way for their use in medical science, such as being the carrier of medical isotopes, or modifying the fullerene to allow it to be water soluble or to increase image quality for MRI [7].

Fullerenes are also of astrophysical significance. Kroto and collaborators [1] were originally simulating carbon star emission spectra in the laboratory when C_{60} was discovered. Many groups spent time looking for the infrared (IR) signature of C_{60} in planetary nebulae, but the first extra-terrestrial (ET) evidence of C_{60} was reported by Becker *et al.* [3] as stated previously. In November, 2010, using data from the Spitzer telescope, Garcia-Hernandez *et al.* [4] reported the IR signature of C_{60} and C_{70} in planetary nebulae. What is strange about this finding is that the fullerenes were detected in hydrogen-rich environments. They concluded that the fullerenes must exist as solids in dust particles located inside the nebulae.

Chapter 2

Theoretical Background

2.1 Introduction

The development of quantum theory at the beginning of the 20th century opened the scientific world to new discoveries and a new way to express phenomena not able to be fully explained or understood using classical physics. Quantum theory challenged classical laws and ultimately showed that they broke down on the atomic and molecular scale. One revolutionary idea that came out of quantum theory was the wave-particle properties of light and matter.

This principle was developed to help explain the results from the photoelectric effect, for which Einstein won the Nobel Prize in 1921. In the photoelectric effect, electrons were ejected from matter after absorbing electromagnetic radiation with an energy ranging from a few eV to over a MeV. The photoelectric effect has opened the door to a field of research that is still active today: the study of photoionization processes.

2.2 Photoionization

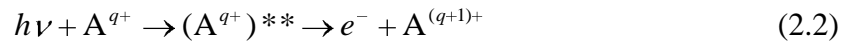
Photoionization is a fundamental process in the universe [8]. It is an important process in high temperature plasmas, such as stars and nebulae, and in inertial confinement fusion. Photoionization measurements give insight into the ionic structure of atoms, molecules, and ions, allowing theorists to build models of multielectron systems and interactions.

Photoionization of atoms, molecules, and ions is a process characterized by a direct photoionization cross section that rises as a step function from zero at the ionization threshold and decreases monotonically with increasing photon energy [8].

This process is represented by:



where h is Planck's constant, ν is the frequency of the photon ($h\nu$ is the energy of the photon), A is the atom or molecule of interest, q is the charge number of the atom or molecule, and e represents an ejected electron. Superimposed upon the direct ionization cross section are resonances at discrete energies representing autoionization states (indirect ionization), characterized as:



where $(A^{q+})^{**}$ is short-lived intermediate state that the ion goes through during the indirect ionization process. Interference between these two ionization processes produces Fano-Beutler line profiles for the resonances, seen in figure 2.1. This can provide insight into the electronic structure of the ion and help characterize the ionization process that occurs. Another type of resonance can occur, which is broad in energy, and involves multiple interacting electrons, known as a giant resonance.

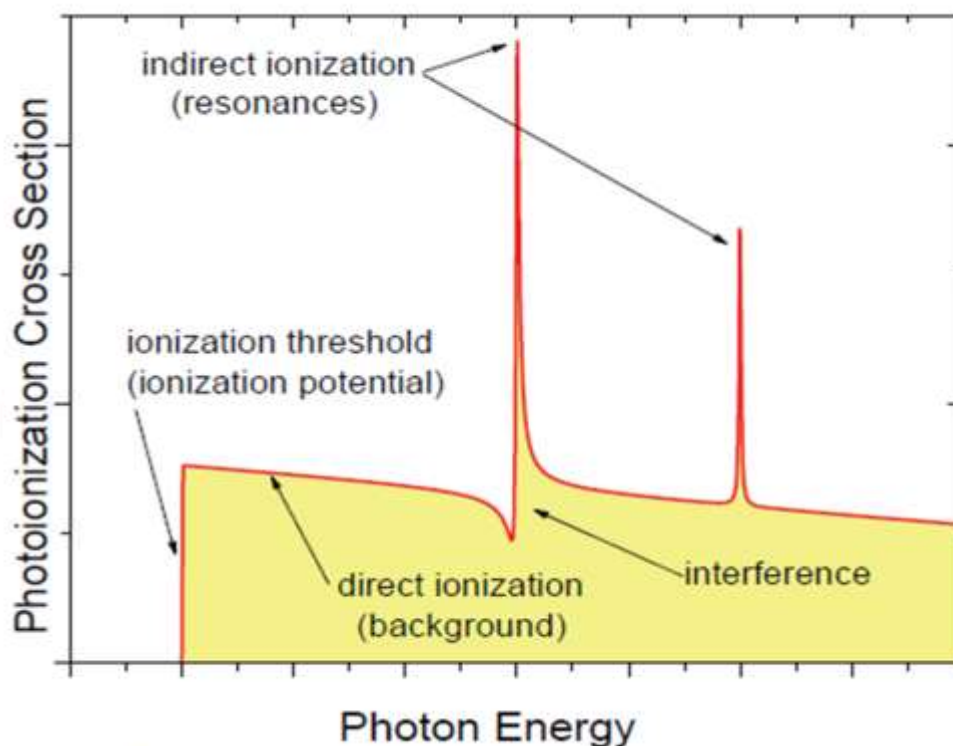


Figure 2.1 Generic photoionization cross section of an atom or atomic ion [9]

2.3 Giant Resonances

Giant resonances were first observed in nuclear physics by Baldwin and Klaiber in 1947 [10]. While conducting experiments for photo-fission in heavy Z elements, giant excitations were observed in their cross sections. While conducting γ -n experiments with ^{12}C and ^{63}Cu later [11], these excitations were once again seen in their cross sections. As explained by Amusia and Connerade [12], these are described using a macroscopic model of the protons oscillating relative to the position of the neutrons in the nucleus.

These giant resonances are not exclusive to the field of nuclear physics; they have also been observed in atomic and molecular systems. A well-known resonance in atomic physics is that observed in the photoionization of the 4d subshell in Xe atoms. This giant resonance corresponds to a $4d \rightarrow \epsilon f$ transition and has an ionization threshold of about 75

eV [13]. These resonances occur in other large Z atoms and their ions with filled 4d subshells, such as Ce [9].

Carbon fullerene photoionization cross sections are dominated, at low energies, by giant resonances. The first giant resonance in free fullerenes, known as the surface plasmon, was first reported by Hertel and collaborators [5] at 22 eV in 1992. This surface plasmon corresponds to a collective motion of the electron cloud about the ionic core [12]. Figure 2.2 compares the giant resonances in the C nucleus, Xe 4d subshell, and C_{60} surface plasmon [12]. It is clear from the figure that a similar physical process governs giant resonances.

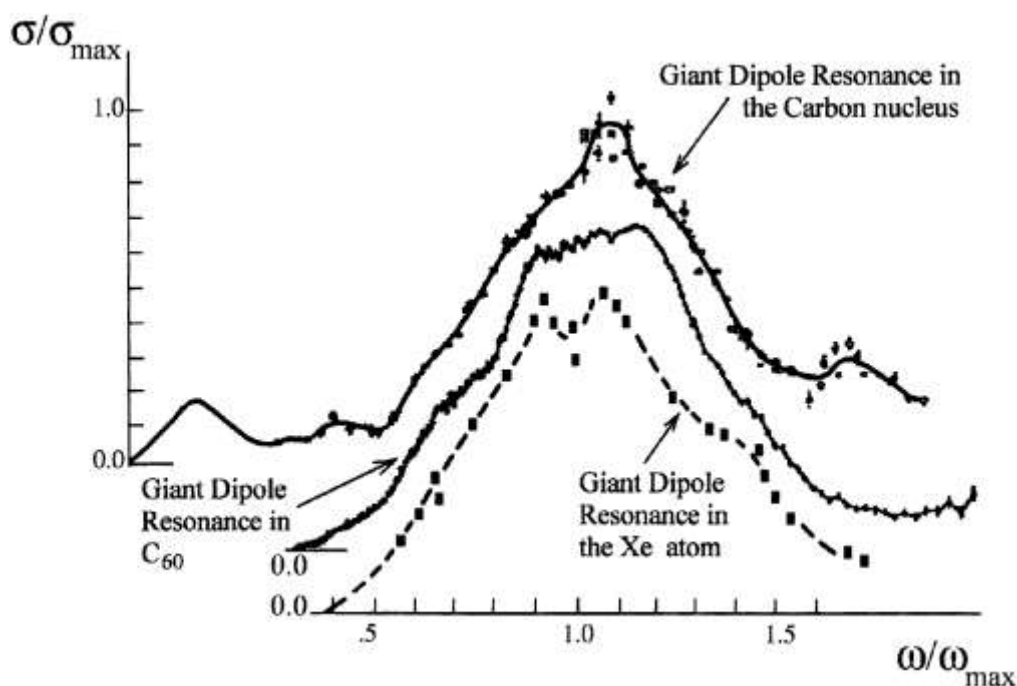


Figure 2.2 Comparison of giant resonances in C nucleus, Xe atom, and C_{60} [12]

A second giant resonance, known as a volume plasmon, was first reported by Scully and collaborators [6] in 2005, occurring around 38 eV. This volume plasmon corresponds to a photon-induced electron-density fluctuation of the delocalized electron cloud. Both plasmons (surface and volume) are electric dipole excited.

Each giant resonance has a finite lifetime τ before it decays and the system relaxes into a lower energy state, for example by ejecting one or more electrons. Its lifetime can be calculated from the uncertainty principle:

$$\tau = \frac{\hbar}{\Gamma} = \frac{h}{2\pi\Gamma} \quad (2.3)$$

where h is Planck's constant ($h = 4.136 \times 10^{-15}$ eVs) and Γ is the full width at half maximum (FWHM) and is measured in units of energy. The value Γ , experimentally, is the real width of the resonance, therefore the broader the resonance, the shorter lifetime it has. For example, in [6], the FWHM of the surface plasmon in the process

$C_{60}^+ + h\nu \rightarrow C_{60}^{2+} + e^-$ is reported as 7.6 ± 0.3 eV, so the lifetime is:

$$\tau = \frac{4.136 \times 10^{-15} \text{ eVs}}{2\pi * 7.6 \text{ eV}} = 8.66 \times 10^{-17} \text{ s.}$$

One can also calculate the frequency of oscillation from the energy of the peak of the resonance by the formula:

$$f = \frac{\omega}{2\pi} = \frac{E_r}{h}, \quad (2.4)$$

where f is the frequency, ω is the angular resonance frequency, and E_r is the energy of the peak of the resonance. E_r was reported as 22.0 ± 0.1 eV, therefore the frequency of oscillation is

$$f = \frac{22.0 \text{ eV}}{4.136 \times 10^{-15} \text{ eVs}} = 5.32 \times 10^{15} \text{ Hz.}$$

With these two values, one can now determine the number of oscillations (N) the resonance experiences before it decays simply by

$$N = \tau f = \frac{E_r}{2\pi\Gamma} \quad (2.5)$$

Scully's numbers give a result of:

$$N = \tau f = 8.66 \times 10^{-17} \text{ s} * 5.32 \times 10^{15} \text{ Hz} = 0.46 \text{ oscillations for the surface plasmon.}$$

Giant resonances can be explained using quantum mechanical potentials.

Connerade uses short-range well potentials and partial waves to construct giant resonance profiles in cross sections [14]. In other cases, classical models can be used. In fact, classical approximations for the plasmons in fullerenes have been used and agree rather well with experiment. A comprehensive study of the plasmons in fullerenes was authored by Phaneuf [15] and a summary will be presented here.

One classical model is Mie scattering. Mie's theory, developed in 1908, was one of the earliest theoretical models used to describe the interaction of small particles and light. Mie solved Maxwell's equations analytically for electromagnetic radiation scattering off tiny conducting metal spheres. It was assumed that these tiny spheres have a positive ion core surrounded by an electron cloud that is loosely bound. The electron cloud responded in a collective fashion to weak external electric fields. A displacement of the electron cloud about the positive ionic core resulted. Simple harmonic motion was able to describe the motion of the electron cloud to the positive core with frequency

(ω_{Mie})

$$\omega_{\text{Mie}} = \sqrt{\frac{n_e e^2}{3\epsilon_0 m_e}}, \quad (2.6)$$

where n_e is the electron density, e is elementary charge, ϵ_0 is the permittivity of free space, and m_e is electron mass. Using the Mie frequency, the surface plasmon energy is predicted to occur at an energy of $\hbar\omega_{\text{Mie}} = 21.4 \text{ eV}$. Scully reported the surface plasmon

in C_{60}^+ to occur, experimentally, at 22.0 ± 0.1 eV [6]. Therefore, Mie scattering describes the mechanism for the surface plasmon quite well.

Another model for describing plasmons is a uniform displacement of an electron gas about a thin metallic slab with displacement of amplitude z perpendicular to the surface. This induces a surface charge of $\sigma = zn_e e$ and an electric field $E = zn_e e / \epsilon_0$. The electric field creates a restoring force, and using Newton's second law, the equation of motion of a unit volume of the gas is simple harmonic motion:

$$n_e m_e \frac{d^2 z}{dt^2} = -n_e e E = -\frac{n_e^2 e^2}{\epsilon_0} z \quad (2.7)$$

$$\frac{d^2 z}{dt^2} + \omega^2 z = 0$$

$$\text{where } \omega = \sqrt{\frac{n_e e^2}{\epsilon_0 m_e}} = \omega_p$$

where ω_p is known as the plasma frequency. If compared to the Mie frequency, then

$$\omega_p = \sqrt{3} \omega_{Mie} \quad (2.8)$$

and $\hbar \omega_p = \sqrt{3} \hbar \omega_{Mie} = 37.1$ eV, compared to 38 ± 2 eV reported by Scully *et al.* [6]. These two simple classical approximations agree surprisingly well with previously reported experimental data.

Giant resonances are natural phenomena that occur in many different physical systems, such as nuclei and molecules, when photoabsorption takes place. The giant resonance can give insight into the collective excitation of strongly correlated particles. After some lifetime τ , they can decay by many different pathways.

Giant resonances in cross sections of nuclei, atoms, and molecules can tell us much about how these systems decay after photoabsorption occurs. For instance, the

giant 4d resonance in Xe has a higher absolute cross section value and greater relative oscillator strength in the double ionization channel than in single ionization [13]. This means that double ionization is more probable for the decay of the resonance in Xe atoms and ions. A comprehensive study of giant resonances in different systems is given by Amusia *et al.* [12].

Oscillator strength, a dimensionless quantity, measures the likelihood of photoabsorption [15]. It can be expressed as:

$$f_{ik} = \frac{g_k}{g_i} \frac{m_e c \epsilon_0 \lambda^2}{2\pi e^2} A_{ik}, \quad (2.9)$$

where f_{ik} is the oscillator strength from initial state i to final state k , g_i and g_k are the statistical weights of the initial and final states, respectively, c is the speed of light, and A_{ik} is the Einstein transition rate. In terms of the fullerene molecules, the cross section can be expressed in terms of a differential oscillator strength per unit energy (eV^{-1}) [9]:

$$\sigma(E) = (2\pi a_0)^2 \alpha R \frac{df}{dE} = 109.7618 \frac{df}{dE} \quad (2.10)$$

where a_0 is the Bohr radius (m), α is the fine structure constant ($\sim 1/137$), and R is the Rydberg constant (m^{-1}). By solving this first order differential equation, one can obtain the average oscillator strength between two energies E_1 and E_2 :

$$\bar{f}_{12} = 9.1106 \times 10^{-3} \int_{E_1}^{E_2} \sigma(E) dE \quad (2.11)$$

By comparing the relative oscillator strengths in several channels, one can deduce which decay modes are preferred. In atomic physics, the sum of the relative oscillator strengths should be equal to the number of electrons involved in the giant resonance [16]. For example, looking at the decay modes of the 4d Xe giant resonances, the total

photoabsorption oscillator strengths should be 10, since Xe has a filled 4d subshell, which contains 10 equivalent electrons.

2.4 Geometry of Fullerenes

Fullerenes consist of 20 or more carbon atoms that are oriented in a closed pattern.

Those with spherical geometry (those with 60 or less carbon atoms) look similar to a soccer ball, while those with more than 60 carbon atoms become prolate and as more carbon atoms are attached, the fullerene will eventually approach the configuration of a cylindrical carbon nanotube. All fullerenes consist of 12 pentagons and m hexagons, where m is given by Euler's formula:

$$m = \frac{n - 20}{2}, \quad (2.12)$$

where n is the number of carbon atoms in the fullerene. For example, C_{60} has 12 pentagons and 20 hexagons, as seen in figure 1.1. Its geometry is known as a truncated icosahedron [17]. If one were to take an icosahedron, made completely of equilateral triangles and cut off the 12 vertices, the faces of the resulting polyhedron will be either pentagons or hexagons, and the resulting polyhedron would be a truncated icosahedron.

Many models show fullerenes as highly symmetric objects. This is not the case. Research conducted by Olmstead, from UC Davis, at the ALS has been on characterization of different structural isomers of different fullerenes. Using synchrotron radiation and crystals of fullerenes, she has been able to resolve the geometry of different structural isomers. In figure 2.3, 2 separate structural isomers of C_{90} reported by Yang *et al.* [18] are shown and asymmetric features can be observed.

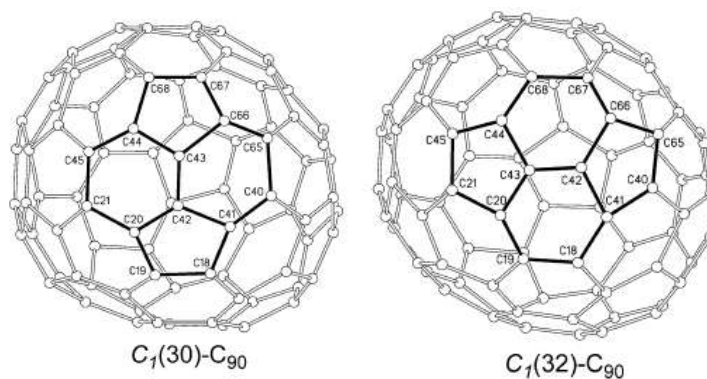


Figure 2.3 Isomers 30 and 32 of C_{90} [18]

Similar research has been conducted by Thilgen and Diederich [19]. They published, in 2006, a comprehensive study of experiments involving structural isomers of many different fullerenes. Figure 2.4 shows two structural isomers, one of C_{68} , another of C_{72} . These structures are less symmetric and are likely present at some level in the ion beams used in the experiments reported in this thesis. Their abundances are unknown, but with the experimental apparatus used (chapter 3), separation or resolution of the different isomers is not possible. This could account for some of the variations in the characteristics of the plasmons measured (chapter 4).

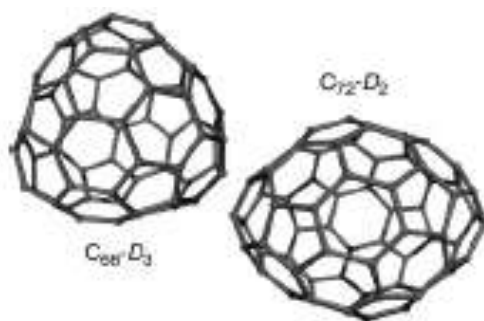


Figure 2.4 Isomers of C_{68} and C_{72} [19]

Chapter 3

Experiment Set-up and Techniques

3.1 Introduction

Experiments for this thesis were performed using a merged-beams technique on beamline 10.0.1 at the Advanced Light Source (ALS) at Lawrence Berkeley National Laboratory (LBNL). The experimental set-up and photoion-yield technique were explained by Covington *et al.* and Habibi [8, 9] and will be summarized in this chapter.

Ions were produced in an electron cyclotron resonance (ECR) ion source, extracted from the ion source by a 6 kV potential difference and electrostatically focused and steered. A 60° dipole analyzing magnet selects a beam of ions based on their mass-to-charge ratio. The ion beam was then merged, using a pair of 90° spherical electrostatic bending plates, onto the axis of a counter-propagating beam of monochromatic synchrotron radiation in an interaction region with an effective length of 29.4 cm. The product ion beam of increased charge is then selected using a 45° charge-analyzing magnet and a pair of 90° spherical deflectors that directs it into a product ion detector. The parent ion beam is directed onto a Faraday cup. Figure 3.1 is a schematic view of the Ion-Photon Beam(IPB) endstation at the ALS beamline 10.0.1.

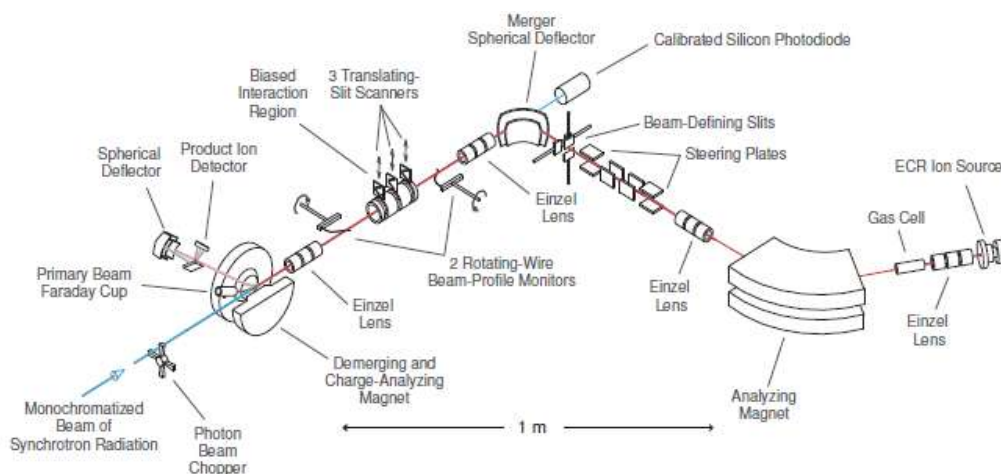


Figure 3.4 Schematic drawing of IPB endstation at ALS beamline 10.0.1 [9]

3.2 Photon Beam

The ALS is a third generation synchrotron radiation source developed at LBNL in 1994, that produces vacuum ultraviolet (VUV) light with very high brightness and photon flux. Electrons are generated from a thermionic gun that is accelerated in bunches by a linear accelerator, then injected into a booster ring where they are further accelerated and injected into a storage ring. In the storage ring, the electrons are accelerated to an energy of 1.9 GeV with a current of 500 mA. Beamline 10.0.1 is served by a 4.55 meter-long undulator with a 10 cm period. The beamline operates over a photon range of 17-360 eV and provides a beam of up to 10^{14} photons/s with high brightness and spectral resolution. Figure 3.2 shows a schematic of the beamline optics.

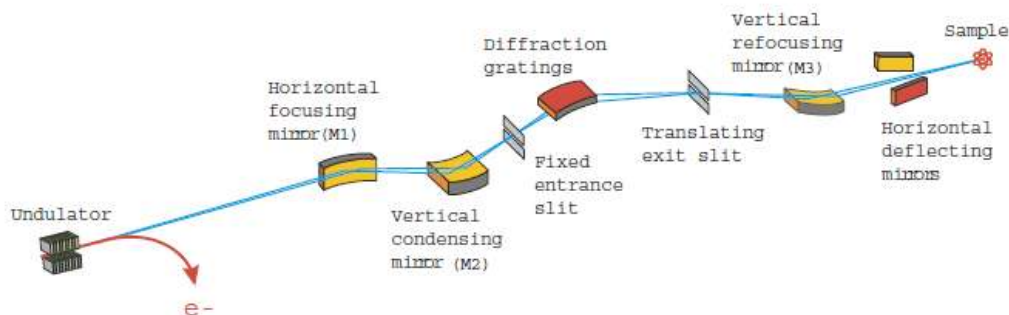


Figure 3.5 Schematic of beamline 10.0.1 optics [9]

Synchrotron radiation from the undulator is focused and directed by a horizontal focusing mirror (M1) followed by a vertical condensing mirror (M2). M2 compresses the beam by a factor of 8, bringing the beam diameter down to less than 1 mm, in order for it to be able to pass through the fixed entrance slit. There are three interchangeable diffraction gratings that allow the user to select the desired energy range for experiments. The low energy grating range is 17-75 eV, medium energy: 40-170 eV, and high energy: 100-360 eV. All experiments for this thesis were performed using the low energy grating. The gratings are designed so that the angle between the entrance and exit slits remains a constant 165° .

In order to scan over a photon energy range, the grating is rotated and the exit slit translated while simultaneously adjusting the undulator gap in order to maximize the intensity of the beam. The entrance and exit slit widths determine the energy resolution. A vertical refocusing mirror (M3) focuses the beam of monochromatic photons and directs it to the endstation.

3.3 Ion Beam

The study of the photoionization of atomic and molecular ions is important because most matter in the Universe is in ionic form [20], so experimental data can be directly applied to observed spectra. Not only that, but ions are much easier to collimate in atomic and molecular physics experiments because they are more susceptible to electric and magnetic fields, so analyzing magnets can be used to select ion beams based on their mass-to-charge ratio, and electrostatic lenses and plates can be used to focus and steer the beam.

The ions used in experiments on the ALS beamline 10.0.1 endstation were created using an ECR ion source, as shown in figure 3.3. Using four permanent ring magnets and 24 permanent magnets arranged in a hexapole configuration, the cyclotron motion of electrons is trapped inside a “magnetic bottle” and is resonantly excited by an external microwave electromagnetic field of frequency 10 GHz [21]. During this process, a plasma discharge is formed and is confined axially by a magnetic mirror created by the ring magnets. The electrons that are removed from the atoms or molecules are radially confined by the hexapole array.

In order to keep the electrons confined in the plasma chamber, the magnetic field intensity (B) near the middle of the chamber was selected to match cyclotron resonance frequency (f_c) for 10 GHz:

$$B = 2\pi \frac{m_e}{e} f_c = 3.58 \text{ kG} \quad (3.1)$$

where m_e is the mass of the electron and e is the charge.

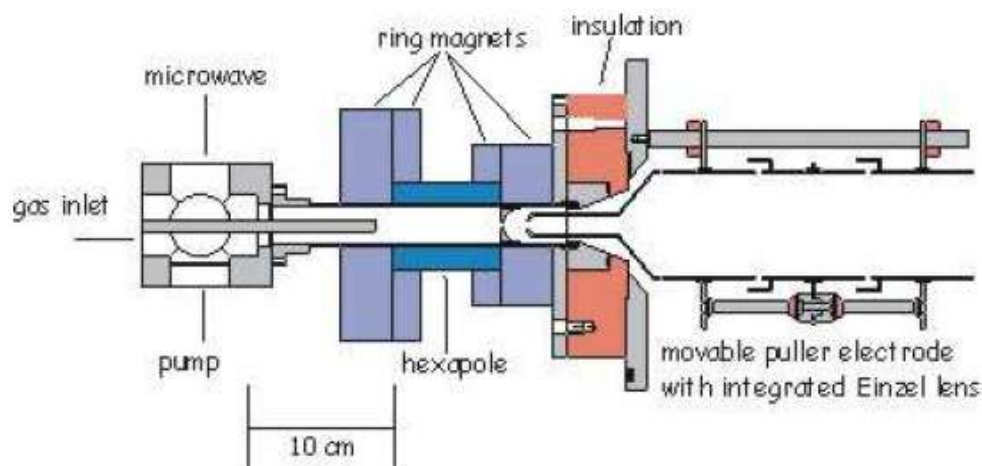


Figure 3.6 Schematic of ECR ion source on IPB endstation [21]

The ion beam is then extracted by a potential difference of 6 kV. It is directed downstream by the use of electrostatic lenses and steering plates and brought on axis to merge with the counter-propagating photon beam. A more detailed description of the ECR ion source is given by Trassl [21].

3.4 Data Collection and Absolute Cross-Section Measurements

After the ion and photon beams interact, they are collected and their intensities are recorded. The photon beam flux is recorded by a NIST calibrated silicon (Si) photodiode at the end of the beamline. The ion beam continues downstream past the interaction region and is deflected out of the plane of the apparatus by a 45° dipole charge analyzing magnet, where it is separated into two beams: the parent ion beam (the beam whose ion charge is unchanged) and the product beam (the beam whose ion charge is of interest).

The parent beam is collected onto a Faraday cup and the current is recorded. The product beam is deflected further by a pair of 90° spherical deflectors into a product ion

detector. Inside the detector, the beam is directed onto a stainless steel plate with a potential of -550V, where secondary electrons are accelerated and detected by a channel electron multiplier used in a pulse-counting mode [8]. This signal is identified as the photoion count rate.

The photon beam varies in energy which is controlled by a computer program, so all photoion signals are recorded as a function of photon energy. This process is known as spectroscopy mode and the photoion spectrum reveals details of the ionic structure. The spectrum can be put on an absolute scale by measuring absolute cross-section values at different photon energies.

Absolute cross-section values can be measured as long as there is a sufficient photoion signal. In fact, the larger the signal, the better the photoion counting statistics and the smaller the error bars are for the absolute value. The absolute cross-section values (σ), as a function of photon energy ($h\nu$) are calculated [8] by:

$$\sigma(h\nu) = \frac{Rqe^2u_i\varepsilon}{I^+I'\Omega\delta\Delta\int F(z)dz}, \quad (3.2)$$

where R is the photoion count rate (Hz), q is the charge of the parent ion beam (for example, C_{60}^+ , $q=1$; C_{70}^{2+} , $q=2$), e is elementary charge (1.6×10^{-19} C), u_i is the ion beam velocity (cm/s), ε is the quantum efficiency of the photodiode (electrons/photon), I^+ and I' are the ion beam and photodiode currents, respectively (A), Ω is the photoion collection efficiency (close to unity), δ is the pulse transmission fraction of the photoion detection electronics (determined by the pulse-discriminator setting), Δ is the measured absolute photoion detection efficiency, and $\int F(z)dz$ is the spatial overlap of the ion and photon beams in the interaction region (cm^{-1}). The form factor $F(z_i)$ is measured in three positions along the interaction region and is calculated by:

$$F(z_i) = \frac{\iint I^+(x, y) I^\gamma(x, y) dx dy}{\iint I^+(x, y) dx dy \iint I^\gamma(x, y) dx dy}. \quad (3.3)$$

Translating-slit scanners are placed at three different positions within the interaction region, one at position z_1 near the entrance, one at z_2 near the middle, and one at z_3 near the end. These slit scanners move over a small spatial range and record the beam intensities of both the ion and photon beams in two orthogonal directions. Since only one-dimensional beam intensity profiles were measured rather than two-dimensional, the approximations:

$$I^+(x, y) = I^+(x) I^+(y) \quad (3.4)$$

$$I^\gamma(x, y) = I^\gamma(x) I^\gamma(y)$$

were taken. Once the three form factors were measured at the three positions z_i along the axis of the interaction region, a 2nd-order polynomial fit was created as an estimation for $F(z)$. Figure 3.4 shows a typical measurement of beam intensities. Figure 3.5 shows a typical fit for $F(z)$ from the three $F(z_i)$ measurements.

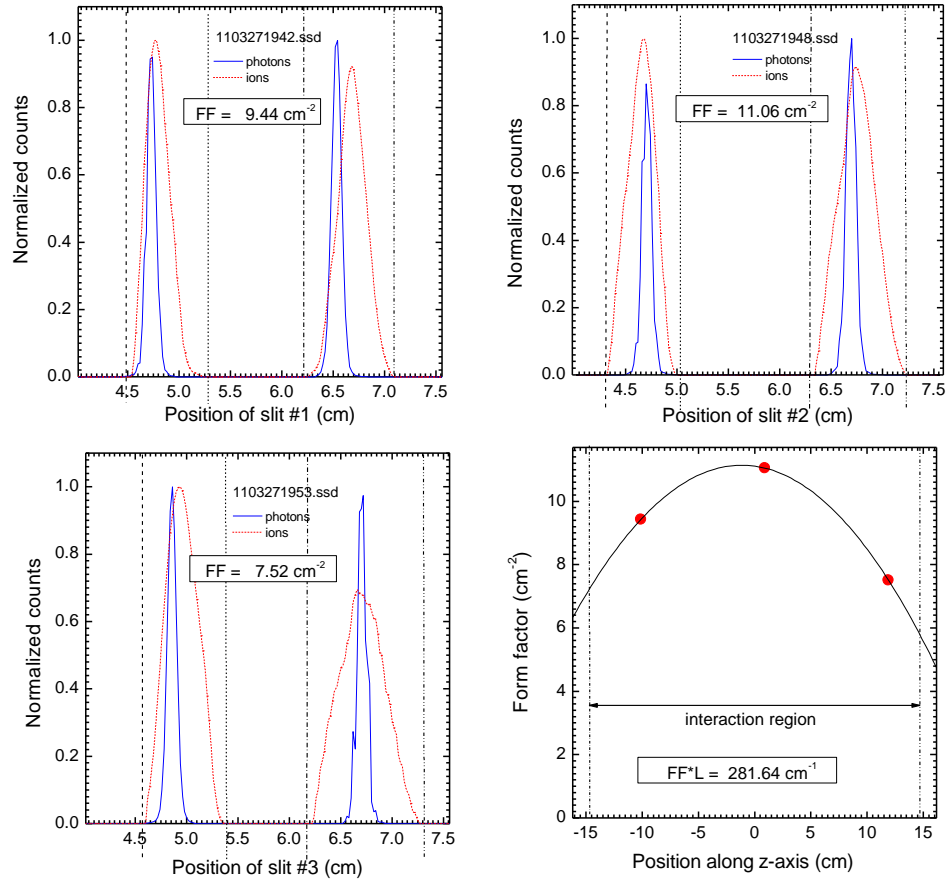


Figure 3.4 Top Left, Right, and Bottom Left: Two-dimensional intensity profiles of the photon beam (solid) and ion beam (dashed). Bottom Right: Polynomial fit of measured form factors to estimate $F(z)$

3.5 Higher-Order Radiation Correction

Higher-order harmonics of the fundamental photon energy are known to be present at the level of several percent on an undulator beamline served by a grating monochromator, but had not been fully characterized on ALS beamline 10.0. In 2010, experiments led by Bilodeau [22] were conducted to quantify this component of the photon flux in order to correct spectra and photon flux measurements when determining absolute cross sections.

Using the well-known ionization thresholds for 2p electrons in Ne (29.950 eV) and 4p in K (18.227 eV or 21.67 eV), these species were photoionized and detected with an electron spectrometer installed on the side branch of beamline 10.0. Three peaks were measured, which corresponded to 1st, 2nd, and 3rd-order radiation. The corrected cross section (σ^{1st}) for 1st- order radiation is given by [22] as:

$$\sigma^{1st} = \frac{qvRQ^{1st}}{I^i FI^p} f = f * \sigma(h\nu) \quad (3.5)$$

where f is a numerical correction factor that is a function of energy. Figure 3.5 shows f as a function of photon energy for a number of photodiodes. The photodiode curve labeled '07 is what is used for corrections to cross-section measurements. For 18 eV, $f = 1.7$ which corresponds to a 70% correction to the measured cross-section. In spectroscopy mode, artifacts from higher order spectra appear at lower energy, but can be removed.

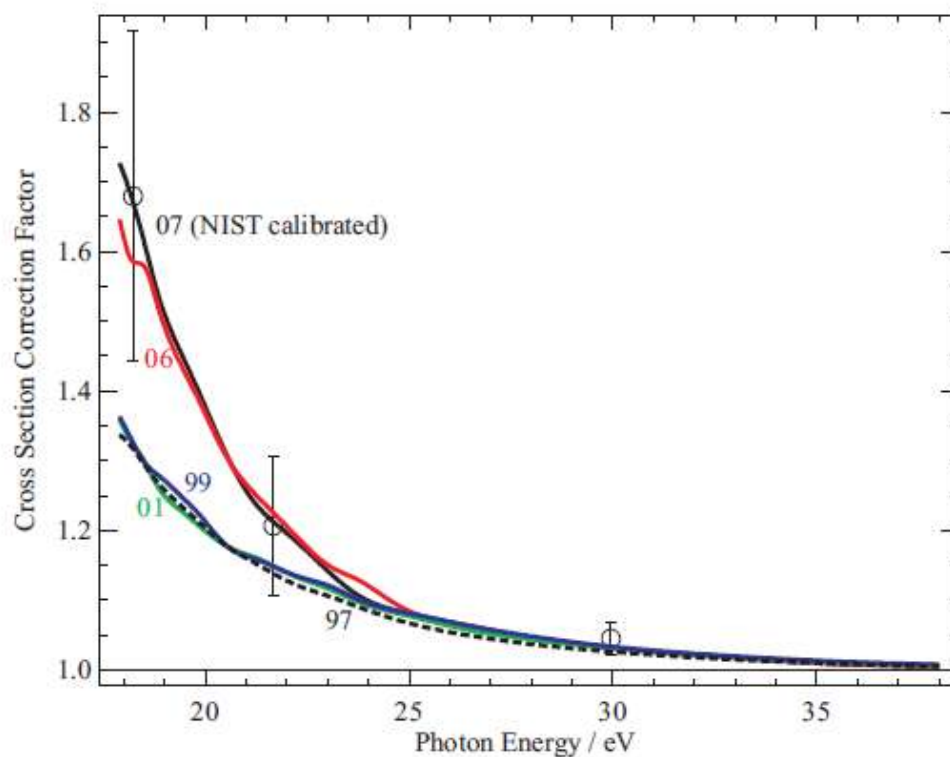


Figure 3.6 Cross-section correction curves for higher-order radiation [22]

Chapter 4

Photoionization of Carbon Fullerene Ions

4.1 Introduction

The experiments reported in this chapter were performed at the ALS. Single ionization cross-section measurements were conducted over the photon energy range of 18-70 eV, with a step size of 0.5 eV, and are represented by $C_n^+ + h\nu \rightarrow C_n^{2+} + e^-$ where n is the number of carbon atoms contained in the fullerene molecule, $h\nu$ is the photon energy, and $n = 40, 50, 60, 70, 76, 78, \text{ and } 84$. The main focus of these experiments was to examine how the characters of the plasmon excitations differ as the value of n was changed.

Once an absolute photoionization cross section was obtained, a fit of the form

$$\sigma(h\nu) = mh\nu + b + \frac{2A_1}{\pi} \frac{\Gamma_1}{4(h\nu - E_{r1})^2 + \Gamma_1^2} + \frac{2A_2}{\pi} \frac{\Gamma_2}{4(h\nu - E_{r2})^2 + \Gamma_2^2} \quad (4.1)$$

was used to fit the two plasmons (Lorentzian fits) which are superimposed on a direct ionization background (linear fit). Once a direct ionization background cross section is determined and parameters m and b are fixed, the advanced fitting tool within Origin 7.5 allows some parameters to be varied and optimized while others are held fixed. Subscript 1 refers to the surface plasmon and subscript 2 to the volume plasmon.

Other quantities that are also of interest and will be discussed with these results are the plasmon lifetimes in seconds, number of oscillations before decay, and their relative oscillator strengths. The Mie and plasma frequencies, eqs (2.6) and (2.8), can

also be estimated from the measured peak energy positions of the surface and volume plasmons, respectively, and comparing the ratio of these quantities to the classical prediction.

Each section in this chapter focuses on a specific fullerene molecular ion and presents the quantities determined as described above. The results of C_{60}^+ photoionization from these experiments and those published by Scully *et al.* [6] are compared and differences between them are analyzed and discussed in section 4.8. A summary and comparison of the parameters for the different fullerene ions are presented in section 4.9.

4.2 Photoionization of C_{40}^+

In its ground state, C_{40} is a closed spherically symmetric molecule, within which the C atoms are arranged as 12 pentagons and 10 hexagons. C_{40} is created in the ECR ion source when C_{60} fragments due to collisions in the microwave discharge. Figure 4.1 presents the photoionization spectrum for $C_{40}^+ + h\nu \rightarrow C_{40}^{2+} + e^-$ normalized to absolute cross-section measurements. The error bars on the absolute points are taken to be $\pm 20\%$ [8]. Forty unique structural isomers of C_{40} have been reported by Fowler *et al.* [23]. With the present experimental method, they could not be resolved from one another and the measurements are assumed to correspond to a mixture of the most stable of these different structural isomers.

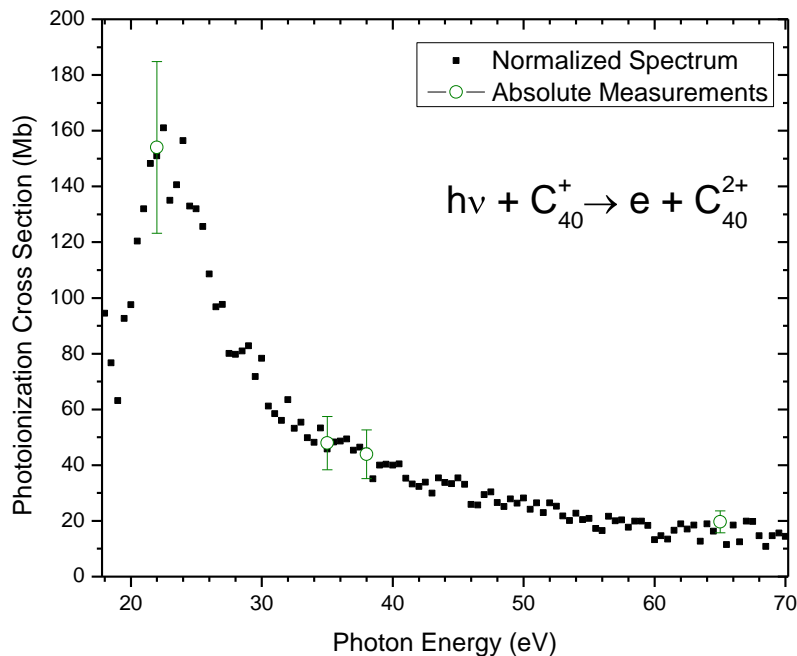


Figure 4.1 Absolute cross-section measurement for single photoionization of C_{40}^+

Using equation 4.1, one can obtain fits for direct ionization and the surface and volume plasmons. Determining the direct ionization background underlying the plasmon features is not a straightforward task. One technique that has been used is to sum the direct ionization cross sections of each individual atom contained in the molecule [24]. For example, using the results of photoionization of neutral C as reported by Hofmann *et al.* [25], the resulting direct ionization cross section of nC is greater than that measured for C_n^+ . Therefore this technique could not be applied to this study. The technique that was used is to assume that direct ionization dominates above 65 eV, so one can extrapolate a linear fit back to zero and use the slope (m) and intercept (b) as the parameters of the direct ionization background for the plasmon fitting.

Figure 4.2 shows the best fit for the plasmons and direct ionization, which was achieved by optimizing several parameters. The values for the peak energy and widths of the plasmons, along with the parameters for the direct ionization (DI) background fit, can be found in table 4.1.

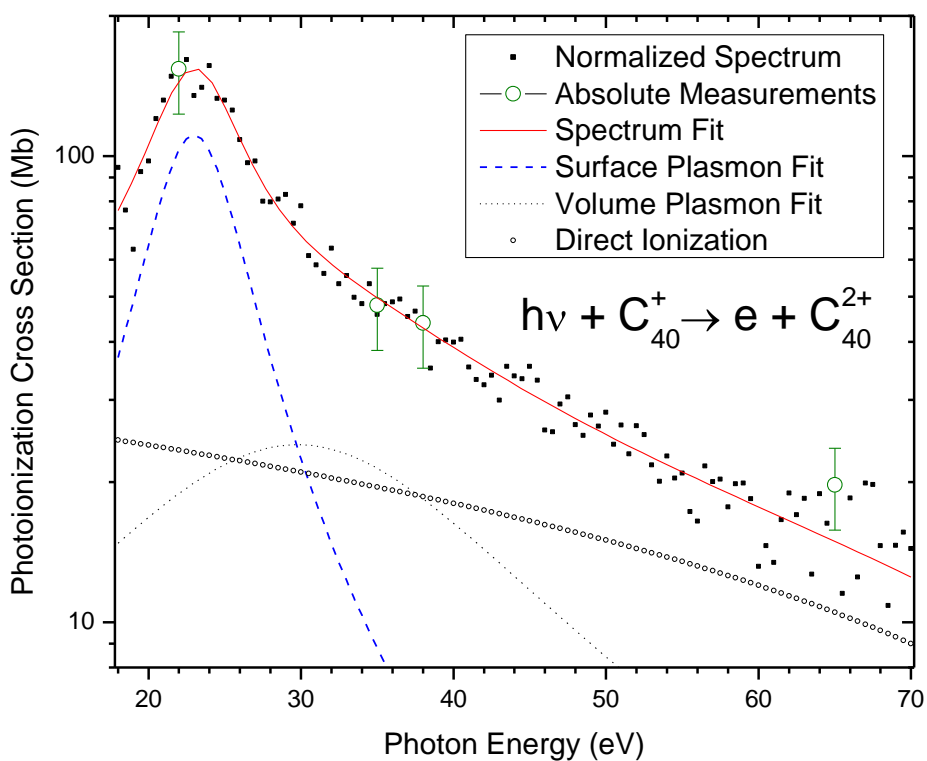


Figure 4.2 Fits of plasmons (Lorentzians) and direct ionization background (linear) to the absolute cross-section measurement of C_{40}^+

Table 4.1 Parameters for C_{40}^+ Fits

Feature	Slope m (Mb/eV)	Intercept b (Mb)	Energy E_r (eV)	Width Γ (eV)
DI	-0.30	30.0		
Surface			23.0±0.1	7.1±0.8
Volume			29.8±4.6	29.8±4.1

Oscillator strengths of resonances can be calculated using equation 2.11. Using the parameterization in equation 4.1, equation 2.11 becomes:

$$\bar{f}_{12} = 9.1106 \times 10^{-3} \int_{E_1}^{E_2} \frac{2A}{\pi} \frac{\Gamma}{4(h\nu - E_r)^2 + \Gamma^2} d(h\nu) \quad (4.2)$$

The DI contribution is not included in equation 4.2 nor is the second Lorentzian because DI plays no role in the plasmon oscillator strength and the two plasmons are treated separately. The indefinite integral of a Lorentzian is:

$$\int \frac{2A}{\pi} \frac{\Gamma}{4(h\nu - E_r)^2 + \Gamma^2} d(h\nu) = \frac{A}{\pi} \tan^{-1} \left(\frac{2(h\nu - E_r)}{\Gamma} \right), \quad (4.3)$$

Using this result, the values given in table 4.1, and the values of the Lorentzian amplitude A , one can calculate the oscillator strengths of each plasmon, where $E_1 = 18$ eV and $E_2 = 70$ eV. The values of A and the oscillator strengths are given in table 4.2. The absolute error bars for the oscillator strengths are taken as $\pm 20\%$, consistent with those of the absolute cross-section measurements.

Knowing the energy peak positions and the widths of each plasmon, one can calculate their lifetimes, both in seconds and in number of oscillations before decay.

Table 4.3 is constructed using equations 2.3 and 2.5.

Table 4.2 Lorentzian Amplitude A and Oscillator Strengths for Surface and Volume Plasmons for C_{40}^+

	Amplitude A (Mb*eV)	Oscillator Strength
Surface Plasmon	1231±229	8.8±1.8
Volume Plasmon	1123±401	6.2±1.3

Table 4.3 Lifetimes of Plasmons for C_{40}^+

	Lifetime (10^{-17} seconds)	Lifetime (number of oscillations)
Surface Plasmon	9.4±1.9	0.52±0.11
Volume Plasmon	2.3±0.5	0.16±0.04

The final parameters to be discussed are the classical Mie and plasma frequencies. It has been demonstrated that the surface and volume plasmon frequencies can be estimated by the classical predictions [6, 15] As described in section 2.3, the ratio of the plasma frequency to the Mie frequency for a conducting sphere is a constant,

$$\frac{\omega_p}{\omega_{Mie}} = \sqrt{3} = 1.73 \quad (4.4)$$

The surface and volume plasmon frequencies may be determined from the fit parameters in table 4.1 and using the equation

$$E_i = \hbar\omega_i \quad (4.5)$$

Table 4.4 lists the frequencies associated with the surface and volume plasmons and their ratio, where ω_s and ω_v represent the surface and volume plasmons, respectively.

Table 4.4 Plasmon Frequency Comparisons for C_{40}^+

ω_s (rad/s)	ω_v (rad/s)	ω_v/ω_s
3.49×10^{16}	4.52×10^{16}	1.30

The following sections consist mostly of similar figures and tables. A comprehensive discussion of all data is presented in section 4.8.

4.3 Photoionization of C_{50}^+

In its ground state, C_{50} is a closed-cage, spherically-symmetric molecule with the C atoms arranged as 12 pentagons and 15 hexagons. Like C_{40} , it is created in the ECR ion source discharge due to fragmentation of C_{60} . Zhao has reported 271 structural isomers of C_{50} [26] and it is likely the C_{50}^+ ion beam consisted of a mixture of the more stable of these isomers. Figure 4.3 presents the photoionization cross section for the process $C_{50}^+ + h\nu \rightarrow C_{50}^{2+} + e^-$. Figure 4.4 shows the best fits for the plasmons and the DI background and table 4.5 lists the fitting parameters.

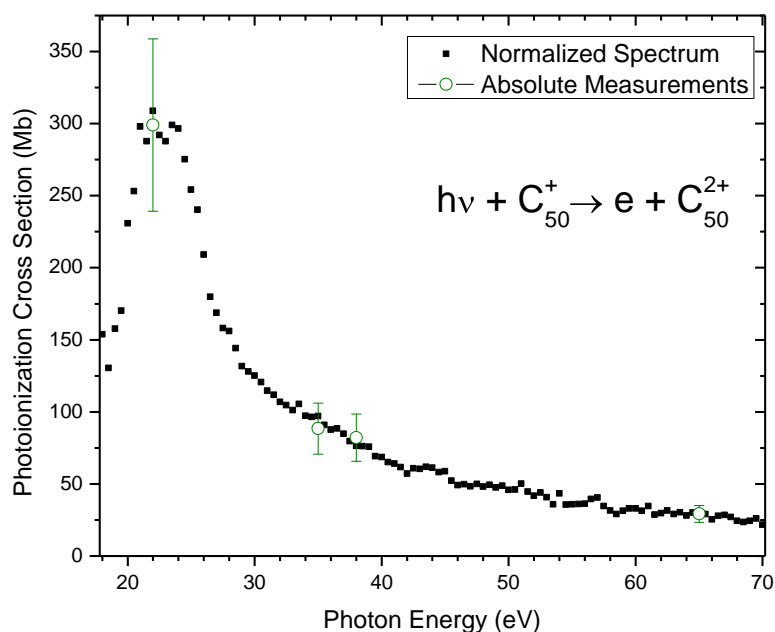


Figure 4.3 Absolute cross-section measurement for the single photoionization of C_{50}^+

Table 4.6 lists the amplitude A and the oscillator strength of each plasmon, table 4.7 lists the lifetimes (seconds, number of oscillations) for each plasmon, and table 4.8 lists the frequencies associated with the surface and volume plasmons and their ratio.

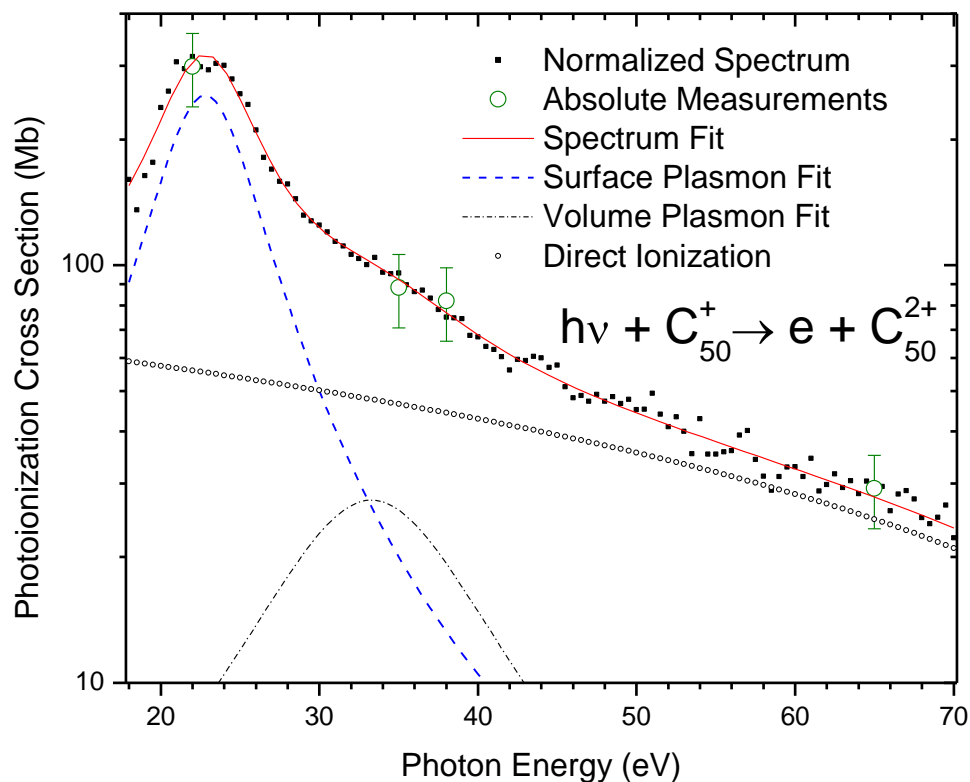


Figure 4.4 Fits of plasmons and direct ionization background for the absolute cross-section measurement of C_{50}^+

Table 4.5 Parameters for C_{50}^+ Fits

Feature	Slope m (Mb/eV)	Intercept b (Mb)	Energy E_r (eV)	Width Γ (eV)
DI	-0.73	71.94		
Surface			22.8 ± 0.1	7.2 ± 0.3
Volume			33.3 ± 1.2	14.6 ± 3.0

Table 4.6 Lorentzian Amplitude A and Oscillator Strengths for Surface and Volume Plasmons for C_{50}^+

	Amplitude A (Mb*eV)	Oscillator Strength
Surface Plasmon	2858±112	20±4
Volume Plasmon	628±138	4.6±1.0

Table 4.7 Lifetimes of Plasmons for C_{50}^+

	Lifetime (10^{-17} seconds)	Lifetime (number of oscillations)
Surface Plasmon	9.3±1.9	0.51±0.11
Volume Plasmon	4.5±0.9	0.37±0.08

Table 4.8 Frequency Comparisons for C_{50}^+

ω_s (rad/s)	ω_v (rad/s)	ω_v/ω_s
3.46×10^{16}	5.06×10^{16}	1.46

4.4 Photoionization of C_{70}^+

C_{70} consists of 12 pentagons and 25 hexagons arranged in a prolate spheroidal geometry.

In these experiments, 99.5% pure C_{60} powder was used, with C_{70} being the other dominant species present. Figure 4.5 shows the ground state geometry of C_{70} . According to the Fullerene Isomer Database [27], 8,149 unique structural isomers of C_{70} have been predicted theoretically.

Figure 4.6 presents the photoionization cross section for the process



Figure 4.7 shows the best fits for the plasmons and DI background. Table 4.9 lists the parameters for energy and width for plasmons, along with the slope and intercept for the DI fit. Table 4.10 lists the amplitude A and the

oscillator strengths for both plasmons. Table 4.11 lists the lifetimes of the plasmons (seconds and numbers of oscillations). Table 4.12 lists the frequencies associated with the surface and volume plasmons and their ratio.

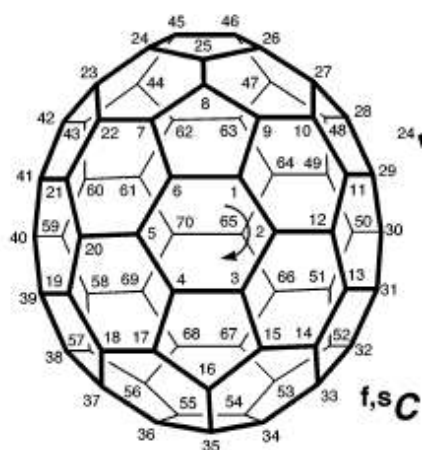


Figure 4.5 C_{70} molecule with carbon numbering [19]

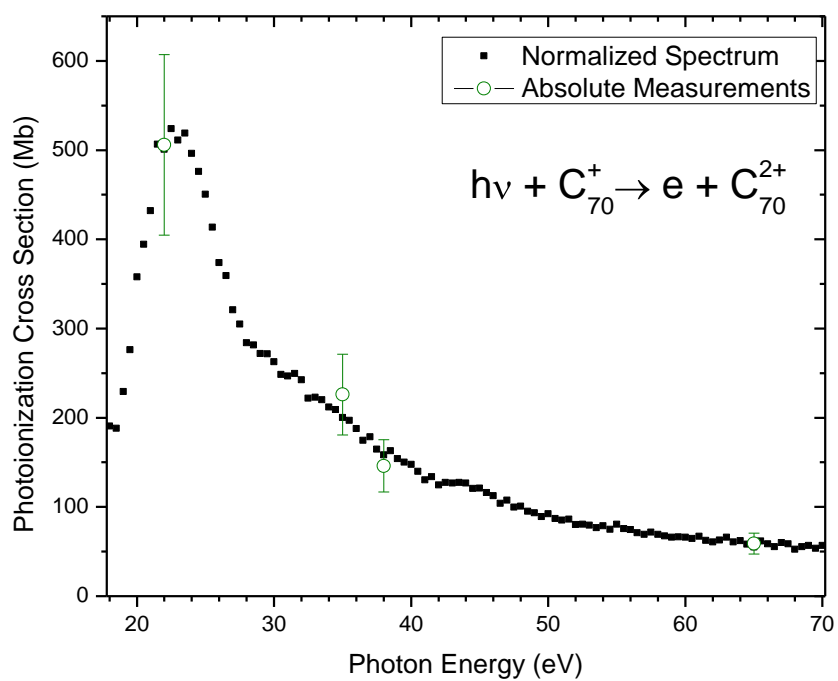


Figure 4.6 Absolute cross-section measurement for the single photoionization of C_{70}^+

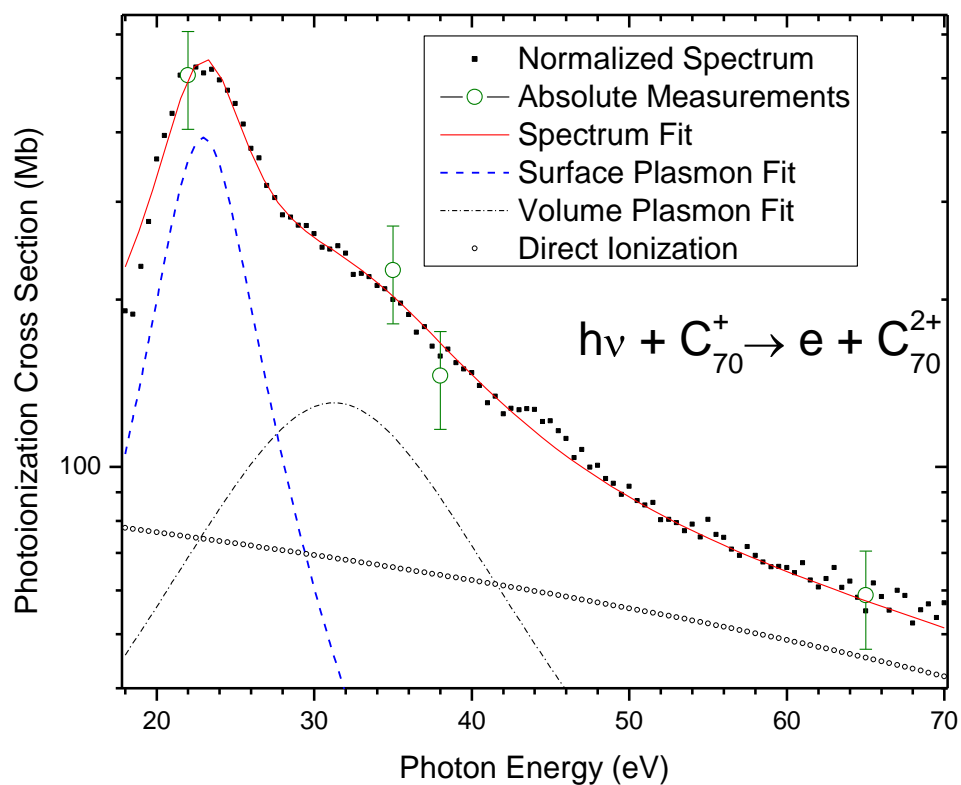


Figure 4.7 Fits of plasmons and direct ionization background for the absolute cross-section measurement of C_{70}^+

Table 4.9 Parameters for C_{70}^+ Fits

Feature	Slope m (Mb/eV)	Intercept b (Mb)	Energy E_r (eV)	Width Γ (eV)
DI	-0.686	90		
Surface			23.0 ± 0.1	6.1 ± 0.3
Volume			31.3 ± 0.8	19.5 ± 1.3

Table 4.10 Lorentzian Amplitude A and Oscillator Strengths for Surface and Volume Plasmons for C_{70}^+

	Amplitude A (Mb*eV)	Oscillator Strength
Surface Plasmon	3706±249	28±6
Volume Plasmon	3998±381	27±6

Table 4.11 Lifetimes of Plasmons for C_{70}^+

	Lifetime (10^{-17} seconds)	Lifetime (number of oscillations)
Surface Plasmon	11.0±2.2	0.61±0.13
Volume Plasmon	3.38±0.68	0.26±0.06

Table 4.12 Frequency Comparisons for C_{70}^+

ω_s (rad/s)	ω_v (rad/s)	ω_v/ω_s
3.49×10^{16}	4.75×10^{16}	1.36

4.5 Photoionization of C_{76}^+

C_{76} consists of 12 pentagons and 28 hexagons. Experiments with higher-order fullerenes ($n > 70$) were conducted using a powder that contained 33% C_{76} , 33% C_{78} , and 33% C_{84} .

C_{76} , along with the other higher-order fullerenes, are similar in geometry to C_{70} , but more prolate. C_{76} is predicted to have 19,151 structural isomers [28].

Figure 4.8 presents the photoionization cross section for the process



Figure 4.9 shows the best fits for the plasmons and DI background. Table 4.13 lists the parameters for energies and widths of the plasmons, along with the slope and intercept for the DI fit. Table 4.14 lists the amplitude A and the oscillator strengths for both plasmons. Table 4.15 lists the lifetimes of the plasmons

(seconds and numbers of oscillations). Table 4.16 lists the frequencies associated with the surface and volume plasmons and their ratio.

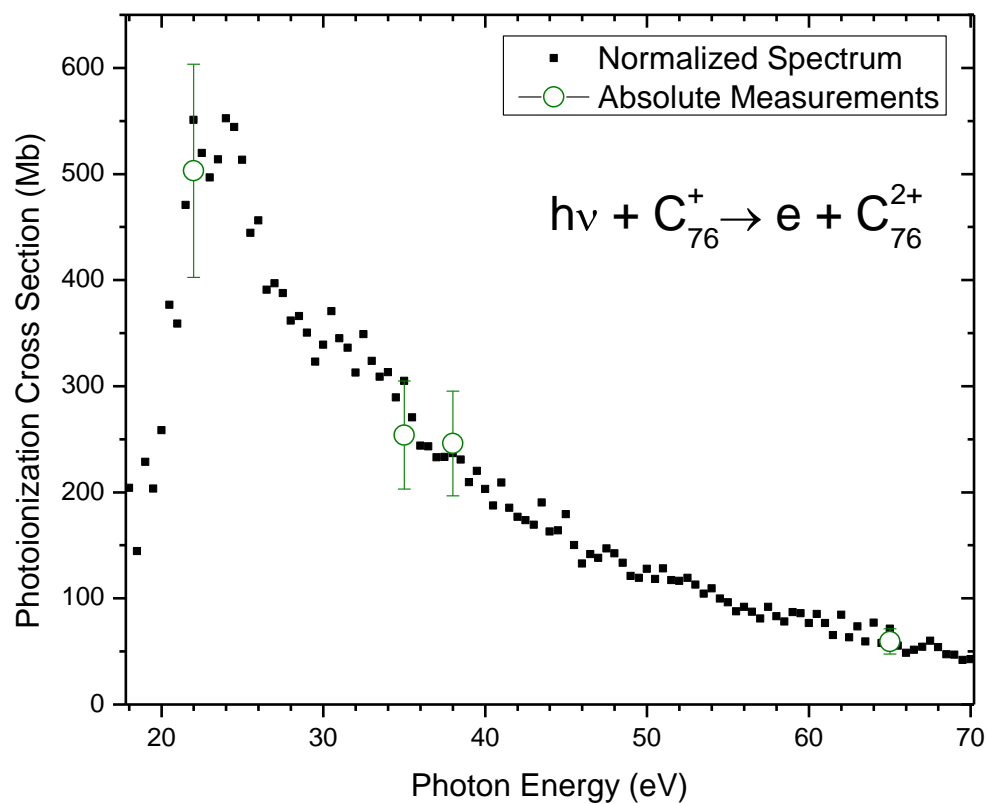


Figure 4.8 Absolute cross-section measurement for the single photoionization of C_{76}^+

Table 4.13 Parameters for C_{76}^+ Fits

Feature	Slope m (Mb/eV)	Intercept b (Mb)	Energy E_r (eV)	Width Γ (eV)
DI	-1.52	148		
Surface			23.54 ± 0.10	5.09 ± 0.49
Volume			31.89 ± 0.72	17.70 ± 1.39

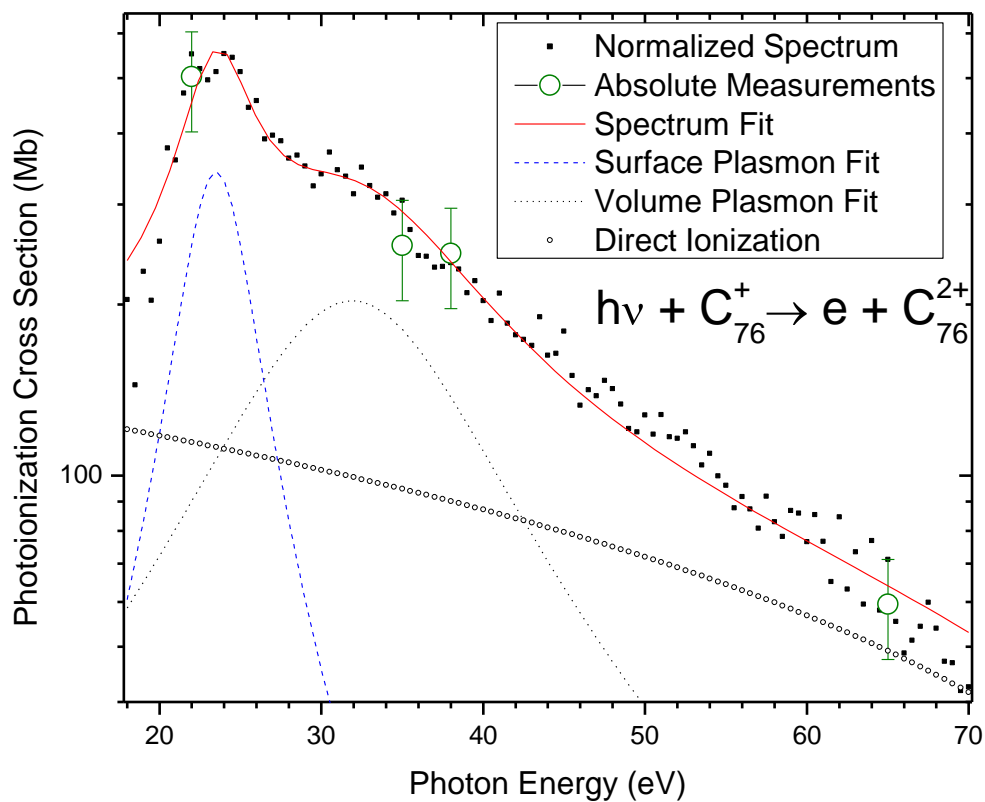


Figure 4.9 Fits of plasmons and direct ionization background for the absolute cross-section measurement of C_{76}^+

Table 4.14 Lorentzian Amplitude A and Oscillator Strengths for Surface and Volume Plasmons for C_{76}^+

	Amplitude A (Mb*eV)	Oscillator Strength
Surface Plasmon	2746 ± 345	22 ± 5
Volume Plasmon	5643 ± 556	39 ± 8

Table 4.15 Lifetimes of Plasmons for C_{76}^+

	Lifetime (10^{-17} seconds)	Lifetime (number of oscillations)
Surface Plasmon	13.0 ± 2.6	0.74 ± 0.15
Volume Plasmon	3.8 ± 0.8	0.29 ± 0.06

Table 4.16 Frequency Comparisons for C_{76}^+

ω_s (rad/s)	ω_v (rad/s)	ω_v/ω_s
3.58×10^{16}	4.84×10^{16}	1.36

4.6 Photoionization of C_{78}^+

C_{78} consists of 12 pentagons and 29 hexagons. C_{78} makes up 1/3 of the powder that was used in these higher-order fullerene experiments. C_{78} is also expected to have numerous structural isomers, but a literature search did not provide a definite number.

Figure 4.10 presents the photoionization cross section for the process



Figure 4.11 shows the best fits for the plasmons and DI background. Table 4.17 lists the parameters for energy and width for plasmons, along with the slope and intercept for the DI fit. Table 4.18 lists the amplitude A and the oscillator strengths for both plasmons. Table 4.19 lists the lifetimes of the plasmons (seconds and numbers of oscillations). Table 4.20 lists the frequencies associated with the surface and volume plasmons and their ratio.

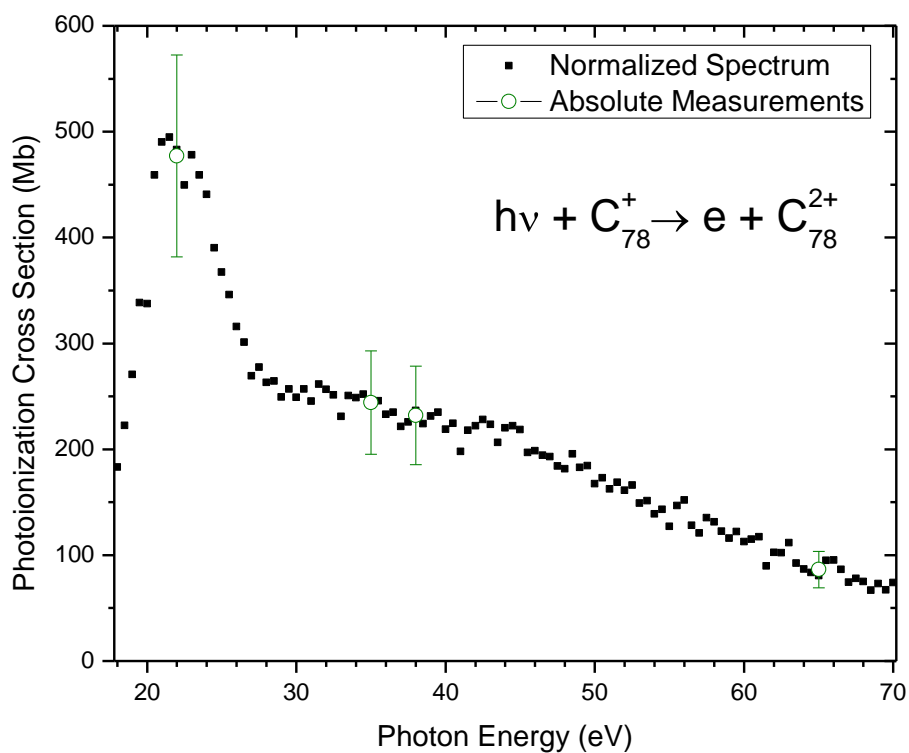


Figure 4.10 Absolute cross-section measurement for the single photoionization of C_{78}^+

Table 4.17 Parameters for C_{78}^+ Fits

Feature	Slope m (Mb/eV)	Intercept b (Mb)	Energy E_r (eV)	Width Γ (eV)
DI	-1.77	152		
Surface			22.4 ± 0.4	5.3 ± 0.4
Volume			39.2 ± 0.9	37.9 ± 2.6

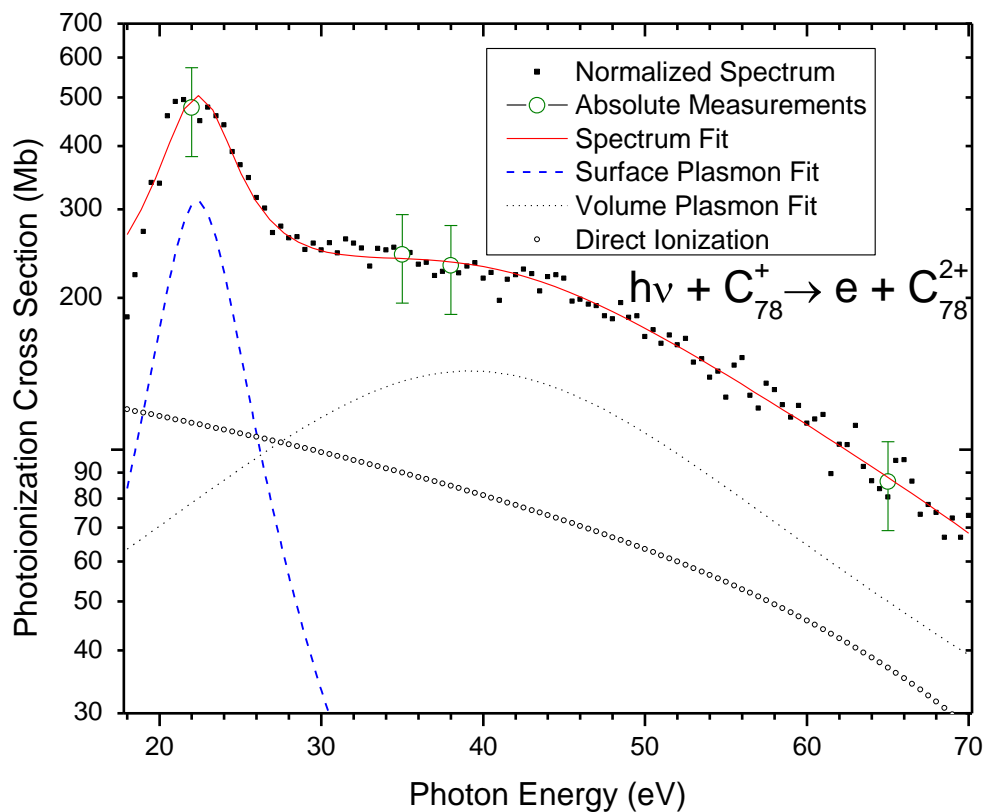


Figure 4.11 Fits of plasmons and direct ionization background for the absolute cross-section measurement of C_{78}^+

Table 4.18 Lorentzian Amplitude A and Oscillator Strengths for Surface and Volume Plasmons for C_{78}^+

	Amplitude A (Mb*eV)	Oscillator Strength
Surface Plasmon	2588 ± 177	19 ± 4
Volume Plasmon	8503 ± 533	46 ± 10

Table 4.19 Lifetimes of Plasmons for C_{78}^+

	Lifetime (10^{-17} seconds)	Lifetime (number of oscillations)
Surface Plasmon	12.5 ± 2.5	0.68 ± 0.14
Volume Plasmon	1.74 ± 0.35	0.17 ± 0.04

Table 4.20 Frequency Comparisons for C_{78}^+

ω_s (rad/s)	ω_v (rad/s)	ω_v/ω_s
3.40×10^{16}	5.95×10^{16}	1.75

4.7 Photoionization of C_{84}^+

C_{84} consists of 12 pentagons and 32 hexagons. C_{84} makes up 1/3 of the powder that was used in these higher-order fullerene experiments. Again, numerous unique structural isomers are expected to exist for C_{84} .

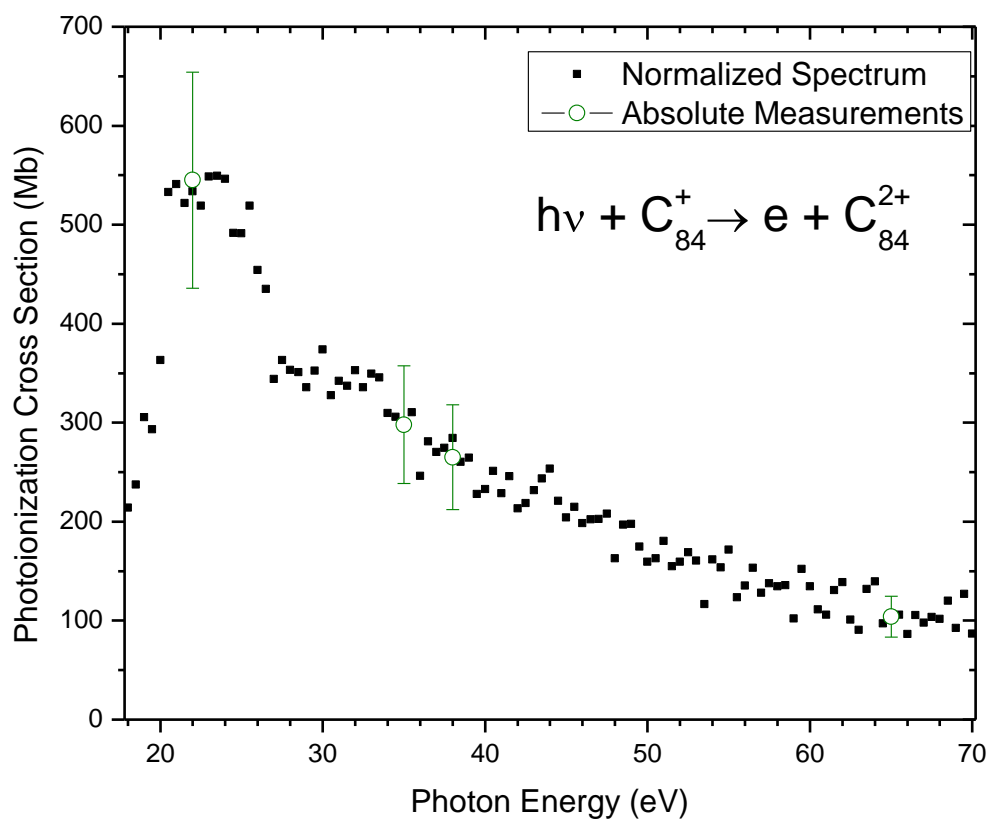


Figure 4.12 Absolute cross-section measurement for the single photoionization of C_{84}^+

Figure 4.12 presents the photoionization cross section for the process $C_{84}^+ + h\nu \rightarrow C_{84}^{2+} + e^-$. Figure 4.13 shows the best fits for the plasmons and DI background. Table 4.21 lists the parameters for energy and width for plasmons, along with the slope and intercept for the DI fit. Table 4.22 lists the amplitude A and the oscillator strengths for both plasmons. Table 4.23 lists the lifetimes of the plasmons (seconds and number of oscillations). Table 4.24 lists the frequencies associated with the surface and volume plasmons and their ratio.

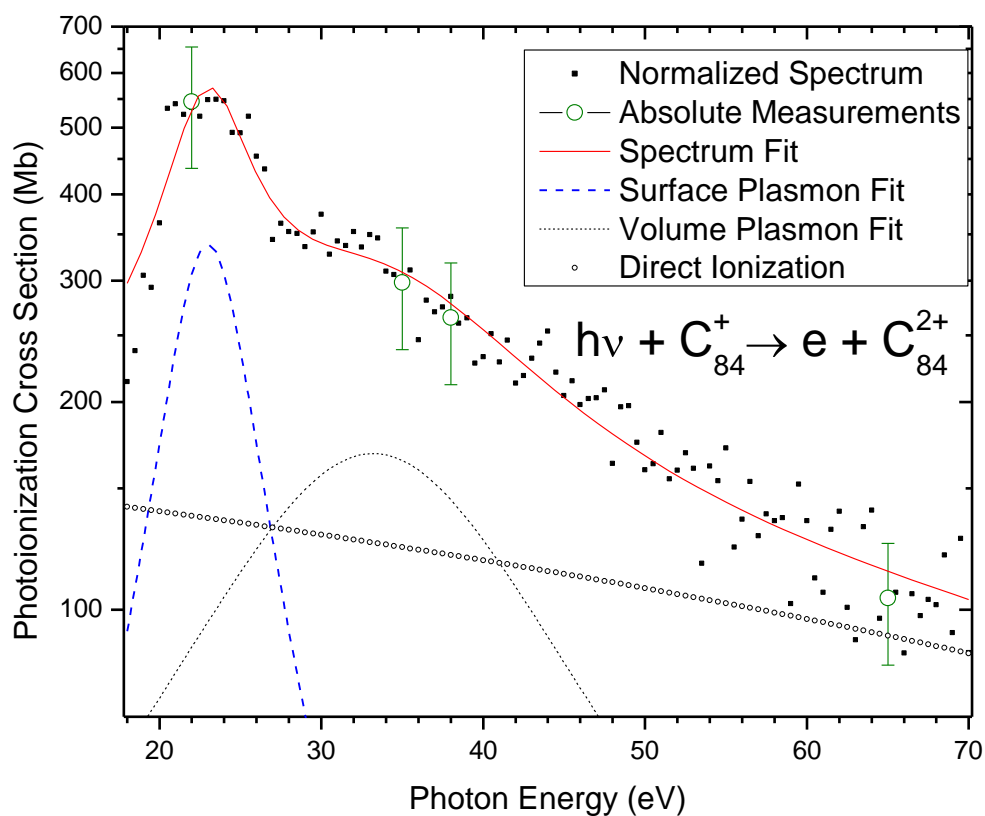


Figure 4.13 Fits of plasmons and direct ionization background for the absolute cross-section measurement of C_{84}^+

Table 4.21 Parameters for C_{84}^+ Fits

Feature	Slope m (Mb/eV)	Intercept b (Mb)	Energy E_r (eV)	Width Γ (eV)
DI	-1.05	160		
Surface			23.0±0.2	6.2±0.8
Volume			33.2±1.5	23.6±4.2

Table 4.22 Lorentzian Amplitude A and Oscillator Strengths for Surface and Volume Plasmons for C_{84}^+

	Amplitude A (Mb*eV)	Oscillator Strength
Surface Plasmon	3277±589	24±5
Volume Plasmon	6220±1420	40±8

Table 4.23 Lifetimes of Plasmons for C_{84}^+

	Lifetime (10^{-17} seconds)	Lifetime (number of oscillations)
Surface Plasmon	10.7±2.2	0.60±0.12
Volume Plasmon	2.80±0.56	0.23±0.05

Table 4.24 Frequency Comparisons for C_{84}^+

ω_s (rad/s)	ω_v (rad/s)	ω_v/ω_s
3.49×10^{16}	5.04×10^{16}	1.45

4.8 Photoionization of C_{60}^+

This next section is divided into two subsections. The first, 4.7.1, consists of the data presented in the same fashion as the previous sections of this chapter. The second, 4.7.2, compares the experimental data from this thesis with the previously published experimental results of Scully *et al.* [6].

4.8.1 Present Measurements

C_{60} is the most well-known, widely studied, and abundant of the carbon fullerenes. Its geometry is described in section 2.4. The Fullerene Isomer Database [27] states that 1,812 unique structural isomers are predicted to exist for C_{60} .

Figure 4.14 presents the photoionization cross section for the process

$C_{60}^+ + h\nu \rightarrow C_{60}^{2+} + e^-$. Figure 4.15 shows the best fits for the plasmons and the DI background.

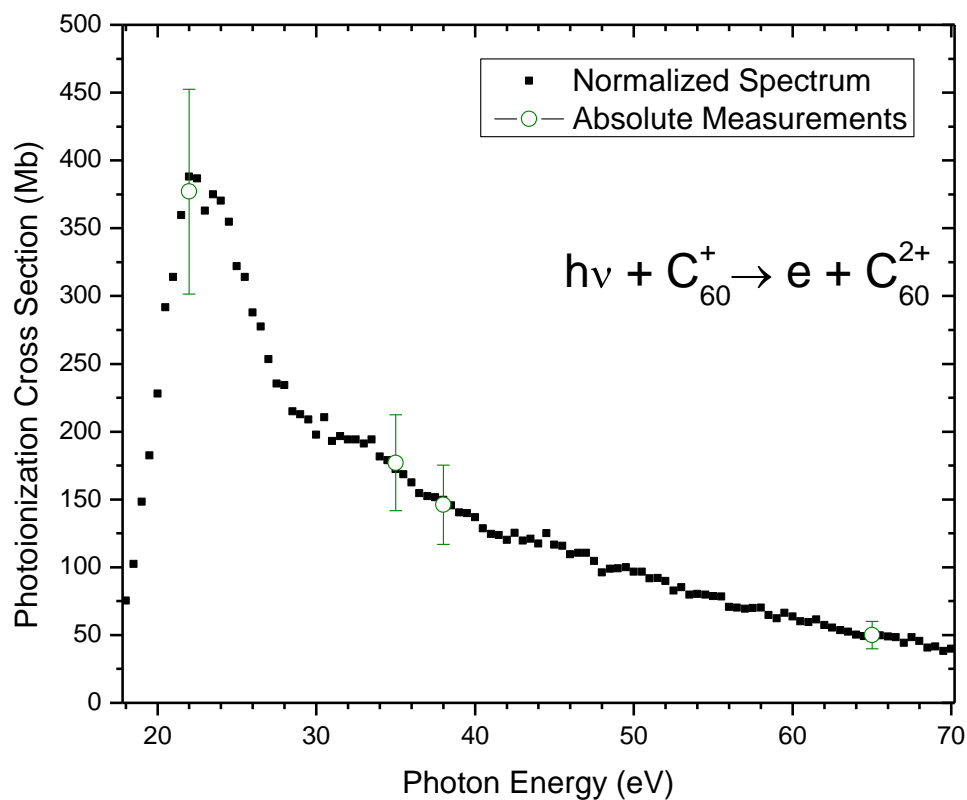


Figure 4.14 Absolute cross-section measurement for the single photoionization of C_{60}^+

Table 4.25 lists the parameters for the plasmon and DI background fits for the single ionization of C_{60}^+ . Table 4.26 lists the amplitude A and the oscillator strengths for both

plasmons. Table 4.27 lists the lifetimes of the plasmons (seconds and numbers of oscillations). Table 4.28 lists the frequencies associated with the surface and volume plasmons and their ratio.

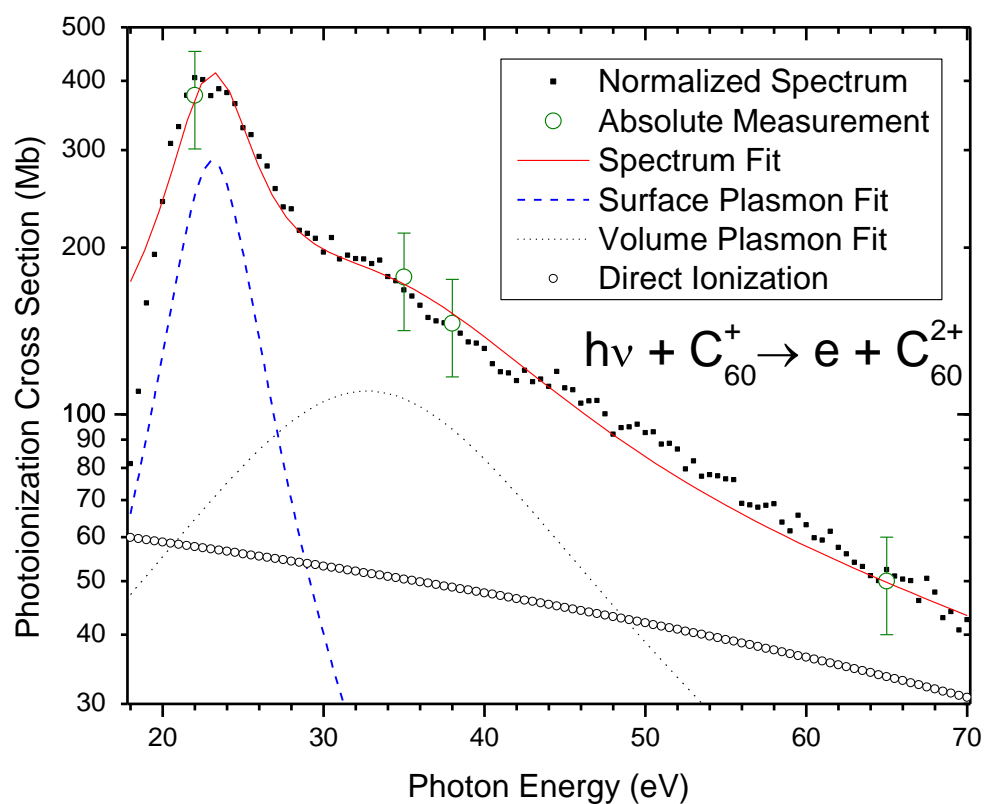


Figure 4.15 Fits of plasmons and direct ionization background for the absolute cross-section measurement of C_{60}^+

Table 4.25 Parameters for C_{60}^+ Fits

Feature	Slope m (Mb/eV)	Intercept b (Mb)	Energy E_r (eV)	Width Γ (eV)
DI	-0.56	70		
Surface			23.1 ± 0.1	5.6 ± 0.5
Volume			32.7 ± 1.4	25.5 ± 2.5

Table 4.26 Lorentzian Amplitude A and Oscillator Strengths for Surface and Volume Plasmons for C_{60}^+

	Amplitude A (Mb*eV)	Oscillator Strength
Surface Plasmon	2514±286	19±4
Volume Plasmon	4413±551	27±6

Table 4.27 Lifetimes of Plasmons for C_{60}^+

	Lifetime (10^{-17} seconds)	Lifetime (number of oscillations)
Surface Plasmon	11.9±2.4	0.66±0.14
Volume Plasmon	2.58±0.52	0.21±0.05

Table 4.28 Frequency Comparisons for C_{60}^+

ω_s (rad/s)	ω_v (rad/s)	ω_v/ω_s
3.51×10^{16}	4.97×10^{16}	1.42

4.8.2 Comparison with Published Data

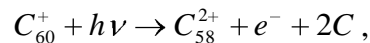
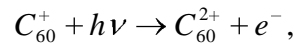
Scully *et al.* [6] first reported the existence of a volume plasmon in the measured photoionization cross section of C_{60} ions in 2005, supported by calculations based on the time-dependent local density approximation. Although initially controversial [29], this discovery and interpretation have now become widely accepted by the theoretical community [30]. Table 4.29 compares the results reported by Scully *et al.* and the present measurements.

Table 4.29 Comparisons of Energy, FWHM, and Oscillator Strengths Reported by Scully *et al.* [6] and Those Presented in this Thesis

	Energy E_r (eV)	Width Γ (eV)	Oscillator Strength
Surface Plasmon [6]	22.0±0.1	7.6±0.3	45±14
Surface Plasmon	23.1±0.1	5.6±0.5	19±4
Volume Plasmon [6]	38±2	29±4	40±12
Volume Plasmon	33±2	26±3	27±6

Comparing the data in table 4.29, the surface plasmon reported values differ by more than their respective error bars. This may be attributable in part to the presence higher-order radiation that was not accounted for in the 2005 experiments (see section 3.4). The surface plasmon feature is most susceptible to the higher-order radiation since it has large correction factors at lower energy (factor of ~1.7 at 18 eV, ~1.3 at 22 eV).

Since the results of C_{60}^{9+} photoionization experiments were reported by Scully *et al.* in 2005, numerous upgrades and modifications have been made to the IPB endstation. One important upgrade has been the installation of a different product ion detector. The detector used for the 2005 experiments contained a larger aperture (diameter = 1.9 cm) than the detector used in the experiments, which is fitted with adjustable slits (diameter \leq 1 cm). Figure 4.16 compares the cross sections for the two processes:



and their sum with the published result [6]. Evidently the sum of the two processes best represents the previously published photoionization cross section. The larger aperture on

the detector that was used for the experiments performed and reported by Scully did not permit resolution of these two product channels.

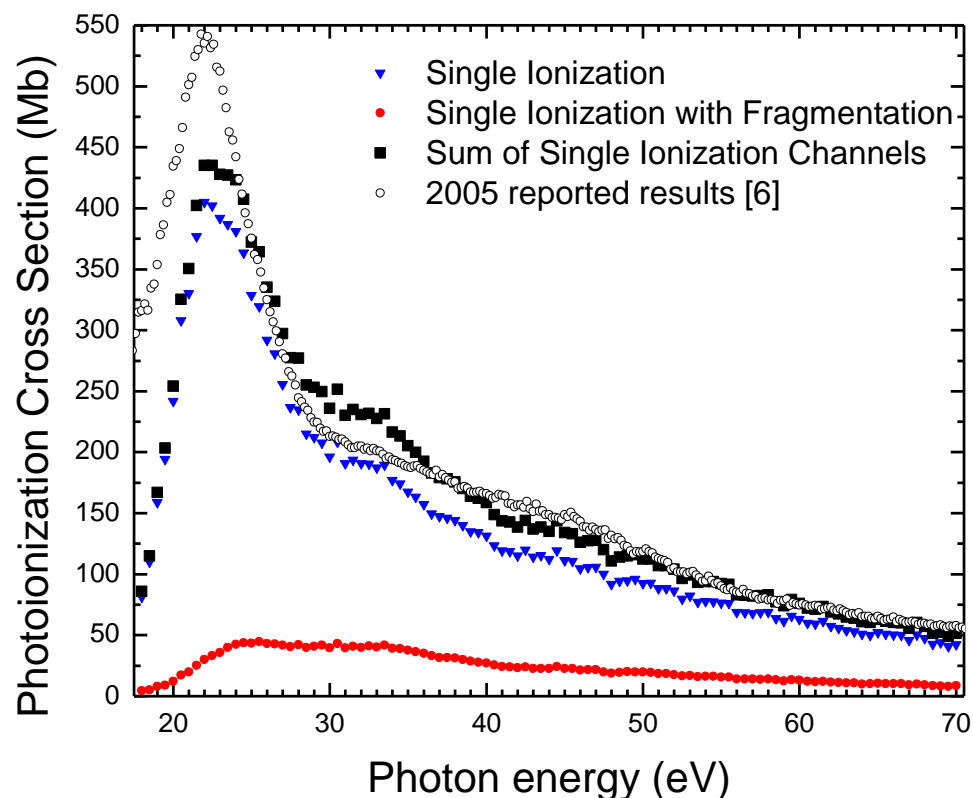


Figure 4.16 Comparison of single photoionization and single photoionization + fragmentation of C_{60}^+

Different photodiodes were used in the experiments conducted by Scully and the experiments reported in this thesis. It was subsequently discovered that the type of photodiode used earlier was susceptible to radiation damage, resulting in an under-recording of the photon flux at energies below 25 eV. As seen in figure 4.17, the flux measured by calibrated type AXUV photodiodes used in previous experiments is compared to that recorded by calibrated type SXUV photodiodes used in subsequent experiments, which are much less susceptible to radiation damage from VUV photon

fluxes delivered by ALS beamline 10.0. From this figure, it is evident that overestimations of the surface plasmon could be attributed to the low photon fluxes measured by the previous photodiodes.

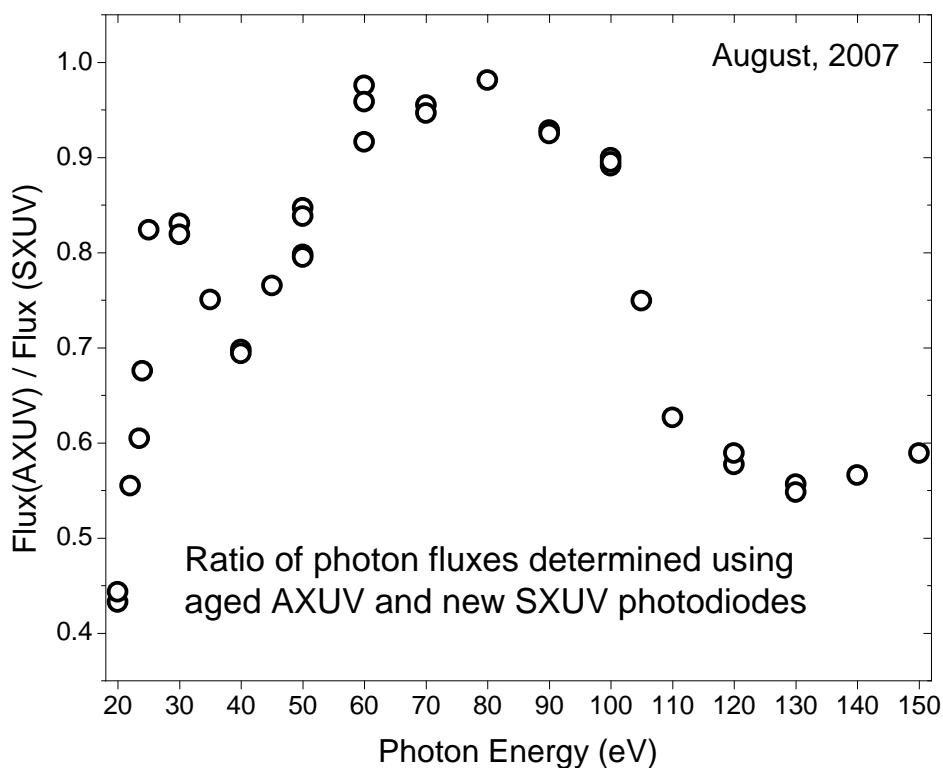


Figure 4.17 Comparison of the photon flux recorded by calibrated photodiodes of different types used in experiments on the IPB endstation

A combination of these effects is likely responsible for their overestimation of the strength of the surface plasmon. It is noted that the present results including both product channels, agree with the published data within their quoted absolute uncertainty over the entire energy range.

Comparing the oscillator strengths in table 4.29, single ionization without fragmentation is evidently not the only decay channel for the plasmons that needs to be

considered. Similar measurements with other fullerene ions [31] indicate that product channels resulting in single or multiple ionization accompanied by fragmentation of pairs of carbon atoms can account for a significant fraction of the total photoabsorption oscillator strength in the VUV.

4.9 Fullerene Comparisons

Throughout this chapter, parameters pertaining to the two photo-excited plasmons in different carbon fullerenes have been presented. The object of this investigation was to investigate the dependence of these parameters on the number of carbon atoms per fullerene molecule.

Quantities of interest are the frequencies associated with the surface and volume plasmon oscillations and their relationships to the classical Mie and plasma frequencies. Comparison of the measured frequency ratios to the classical prediction of $\sqrt{3}$ indicates differences of as much as 25%. All ratios can be found in table 4.30. The Mie scattering model assumes spherical symmetry; however, the higher-order fullerenes are known to be non-spherical. Also, many structural isomers are predicted to exist for each fullerene, whose stabilities and symmetries vary. The primary ion beams for the current experiments undoubtedly contained a mixture of the more stable of these isomers, compromising the applicability of the Mie scattering model to the present measurements.

Table 4.30 Comparison of Volume-to-Surface-Plasmon-Frequencies Ratios for All Fullerenes Reported in This Thesis

N	40	50	60	70	76	78	84
ω_v/ω_s	1.30	1.46	1.42	1.36	1.36	1.75	1.45

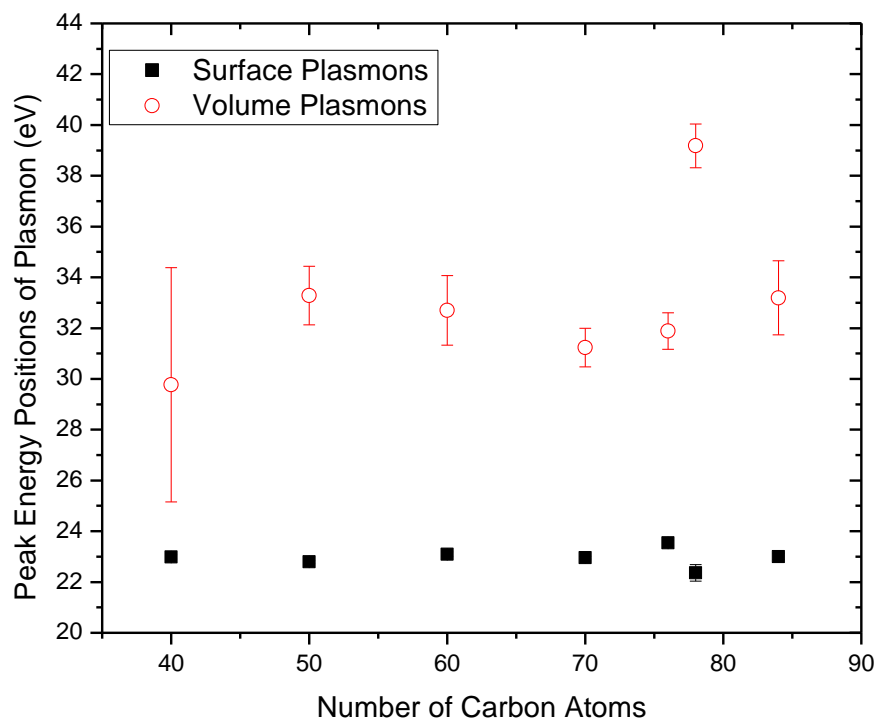


Figure 4.18 Comparison of surface and volume plasmon peak energy positions for the different fullerene molecular ions

Figure 4.18 compares both the surface and volume plasmon peak energy positions as a function of number of carbon atoms. Figure 4.18 compares the widths of both plasmons as a function of number of carbon atoms. Figure 4.19 compares the oscillator strengths of both plasmons as carbon atom number varies. The peak energy positions for the surface plasmons all are within 1 eV of each other. The peak energy positions for the volume plasmons, with the exception of C_{78} , agree within their respective error bars. In the case of C_{78} , there may be one or more possible stable structural isomers whose structure is arranged in a way that causes a shift in the volume plasmon energy position.

However, the present apparatus is unable to distinguish and separate different structural isomers from one another.

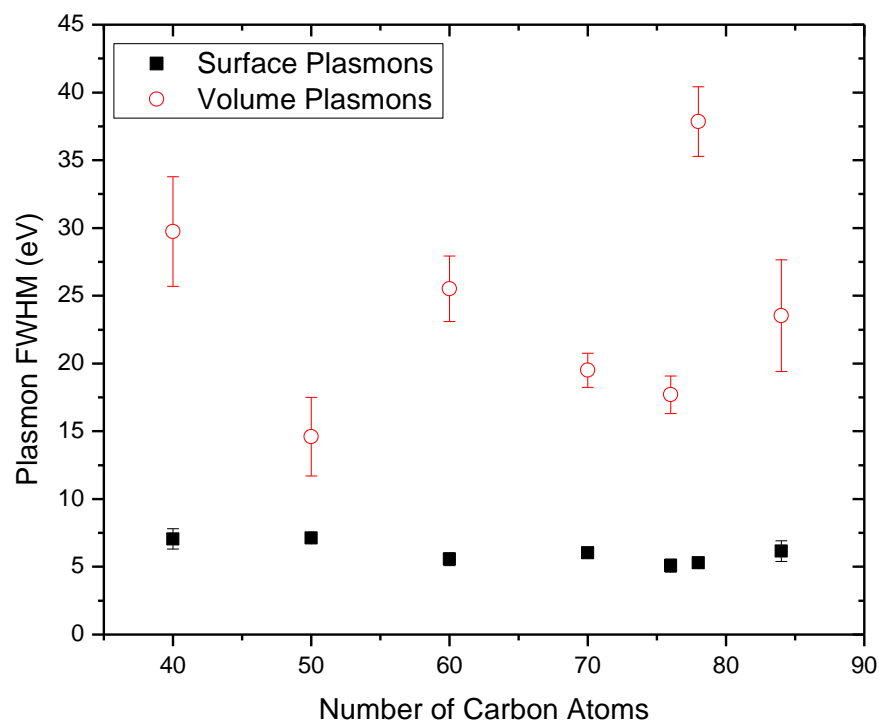


Figure 4.19 Comparison of surface and volume plasmon widths for the different fullerene molecular ions

In figure 4.19, the surface plasmon widths vary little, with the largest values measured for the smaller, more spherically-symmetric fullerenes. This could be a property of their symmetry. The measured widths of the volume plasmons vary greatly, indicating a correspondingly large variation of their plasmon lifetimes. These large variances in the widths may be due to the relative stabilities of different structural isomers present in the samples.

Figure 4.20 indicates that the oscillator strengths of both plasmons increase with the number of carbon atoms, and hence the total number of valence electrons participating in the collective plasmon oscillations.

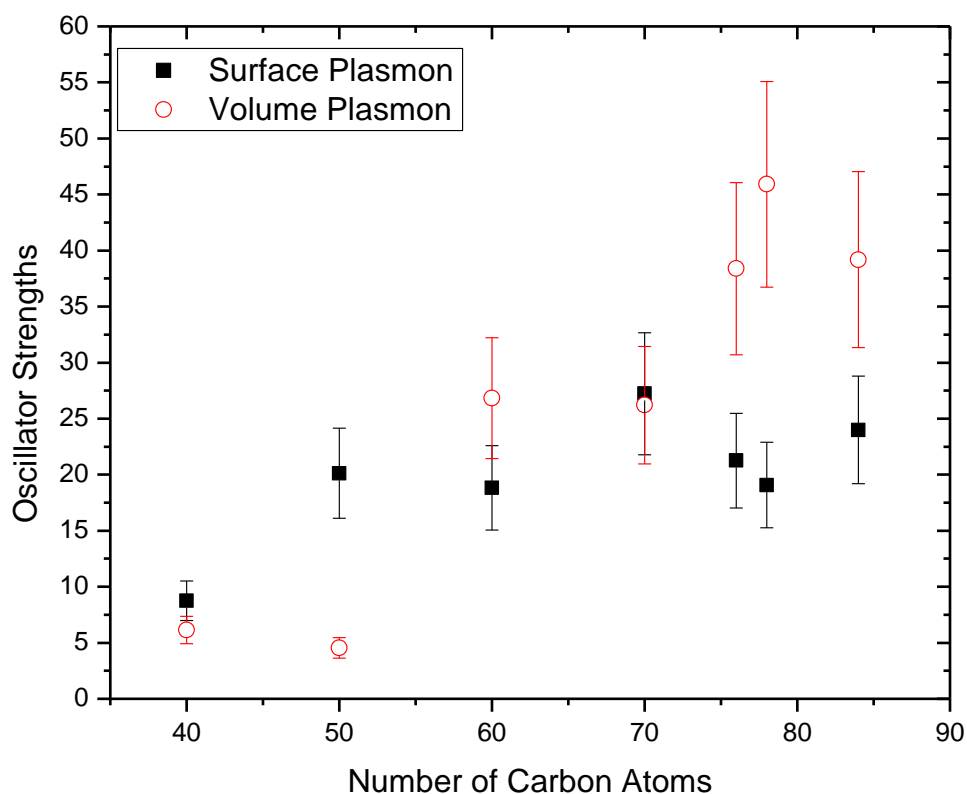


Figure 4.20 Comparison of surface and volume plasmon oscillator strengths for the different fullerene molecular ions

For fullerenes contain 60 or more carbon atoms, the volume plasmon plays a larger role in the ionization process, since the oscillator strengths become greater than those of the surface plasmon.

Figure 4.21 compares the lifetime of the plasmons before decay. The surface plasmon lifetimes agree within their relative error bars because their widths vary little

from fullerene to fullerene, as seen in figure 4.19. The volume plasmon lifetimes agree, for the most part, within their relative error bars, with the exception of C_{78} . Its large width indicates a short mean lifetime, which may be due in part to the relative stability of C_{78}^+ compared to the other fullerene ions studied.

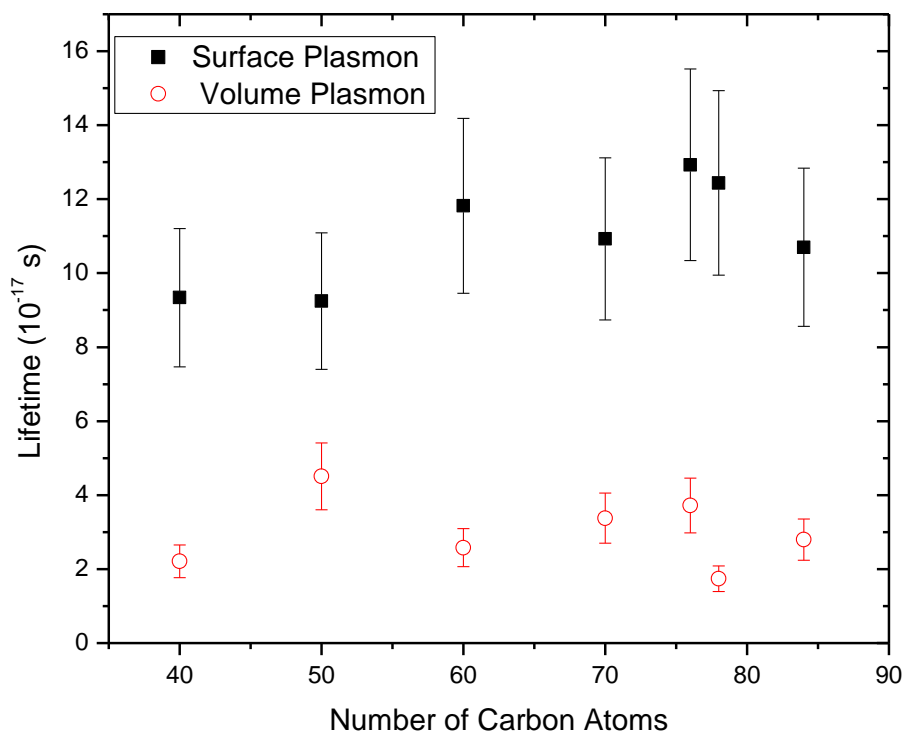


Figure 4.21 Comparison of plasmon lifetimes

Figure 4.22 compares the number of oscillations each plasmon executes before decay. The number of oscillations of the surface plasmons agree with each other agree within their relative error bars, which is to be expected since their peak energies and widths have little variance, much like their lifetimes.

The numbers of oscillations the volume plasmons execute, for the most part, also agree within their error bars. The exception is C_{50} because of its large energy-to-width ratio compared to the other fullerenes.

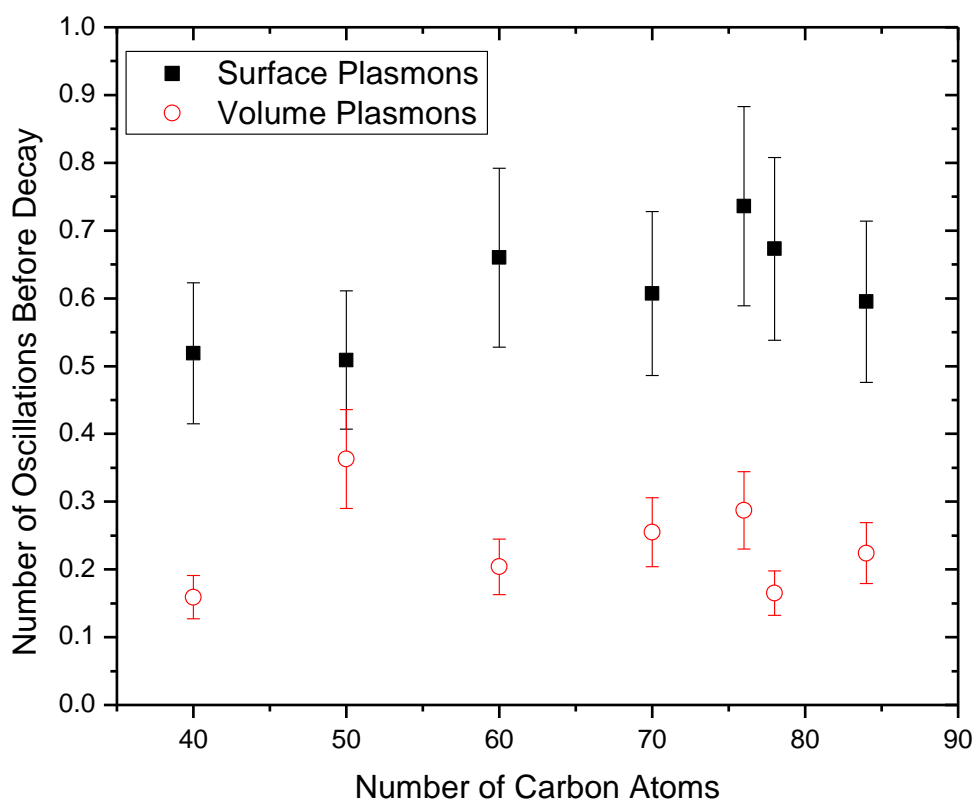


Figure 4.22 Comparison of oscillations each plasmon experiences before decaying

It is evident from these two figures that, with a few exceptions, lifetimes and numbers of oscillations are not strongly dependent on the number of carbon atoms present in the fullerene molecule. However, single ionization is not the only decay mode following VUV photoabsorption. Preliminary experiments have revealed the importance of other decay modes, as discussed in chapter 5.

A noteworthy result that is evident from figure 4.22 is that less than one complete oscillation is executed for all the plasmons studied. This is a general characteristic of giant resonance phenomena observed in nature (e.g. in nuclei, atoms, and molecules, as noted by Amusia *et al.* [12]-see figure 2.2).

Chapter 5

Summary, Conclusions, and Future Work

Photoionization of different fullerene ions was investigated using the IPB endstation on beamline 10.0.1 at the ALS at LBNL. Different physical parameters, such as surface and volume plasmon resonance widths, lifetimes, and oscillator strengths were discussed.

Comparison of the results for C_{60}^+ photoionization with those reported by Scully *et al.* [6] indicate that their measurements corresponded to the unresolved reaction channels



5.1 Summary and Conclusions

Cross-section measurements of the single photoionization of fullerene ions C_n^+ ($n = 40, 50, 60, 70, 76, 78, 84$) were conducted over the photon energy range of 18-70 eV, with a step size of 0.5 eV. Plasmon resonances and the underlying direct ionization component were fitted for all fullerene cross sections using Lorentzian and linear fits, respectively. From the plasmon fits, peak energy positions, widths, and Lorentzian amplitudes were extracted. From these, other quantities of interest, such as oscillator strengths, lifetimes, and number of plasmon oscillations before decay could be calculated.

Many of the physical parameters for the surface plasmons do not vary with carbon number n . In fact, the only physical parameters studied that exhibit significant dependences on n are the surface plasmon oscillator strengths. This also holds, to a lesser

extent, for the volume plasmon. There is more variance among the volume plasmon parameters, which, however, are generally consistent within their uncertainties. The photoionization cross sections and plasmon oscillator strengths increase with n as expected, since the molecular size increases and therefore the likelihood of photoabsorption.

While it is the dominant channel, single ionization is not the only decay mode for the plasmons following VUV photoabsorption. In fact, fragmentation of the fullerene cage can account for a significant fraction of the total photoabsorption oscillator strength at higher photon energies. In the case of C_{60}^+ photoionization, the fragmentation of two carbon atoms from the cage may account for one third of the oscillator strength of the volume plasmons. Figure 5.1 shows quasi-one-dimensional scans of the mass spectra of ionized products resulting from VUV photoabsorption by C_{70}^+ at three discrete photon energies, 22 eV, 35 eV, and 65 eV. They were obtained by simultaneously stepping the demerger magnetic field and the spherical analyzer voltage to direct products of different mass to the ion detector.

Although pure ionization still dominates, fragmentation product channels become relatively more significant at the two higher photon energies. Absorption of a 22 eV photon adds insufficient energy to ionize and fragment a C_{70}^+ ion, since the C-C bond energy is 15.96 eV [32] and the ionization potential is 11.5 eV. The fact that the product scan at 22 eV shows some evidence of fragmentation is a likely indication that some of the primary C_{70}^+ ions were initially in excited isomeric states. Figure 5.1 provides evidence that some decay modes of the volume plasmon include multiple fragmentation.

Other possible decay channels at higher photon energies include multiple ionization and multiple ionization with fragmentation, which were not investigated.

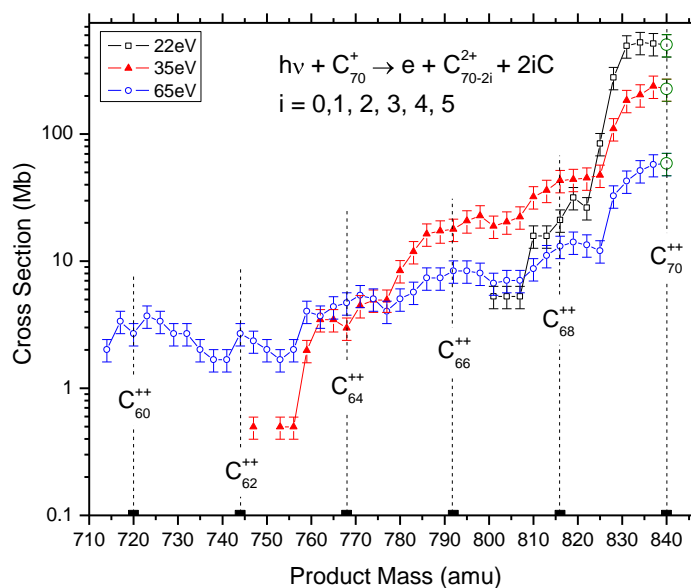


Figure 5.1 Quasi-One-Dimensional Fragmentation Scan of C_{70}^+ at Photon Energies of 22, 35, and 65 eV

The present cross-section measurements have been used to normalize photoionization and photofragmentation measurements with endohedral fullerene ions. Since the ion beam currents with the endohedral fullerenes are extremely low (fractions of pA), it is impossible to characterize the beam overlaps needed to obtain absolute measurements. Cross-section measurements for empty C_n^+ fullerenes may be used to place endohedral fullerene spectra on an absolute scale.

5.2 Future Work

This thesis represents both a comprehensive study of plasmons in single ionization experiments with fullerene ions and suggests some future directions for related research. Fullerene plasmon excitations have multiple decay modes. In Figure 5.2, two-dimensional product ion scan data for the ionization/fragmentation of C_{70}^+ is presented for a fixed photon energy of 22 eV. Such a scan provides a much more comprehensive mapping of the product space and serves as a proof of principle for future experiments involving both single and double ionization of fullerene ions accompanied by fragmentation.

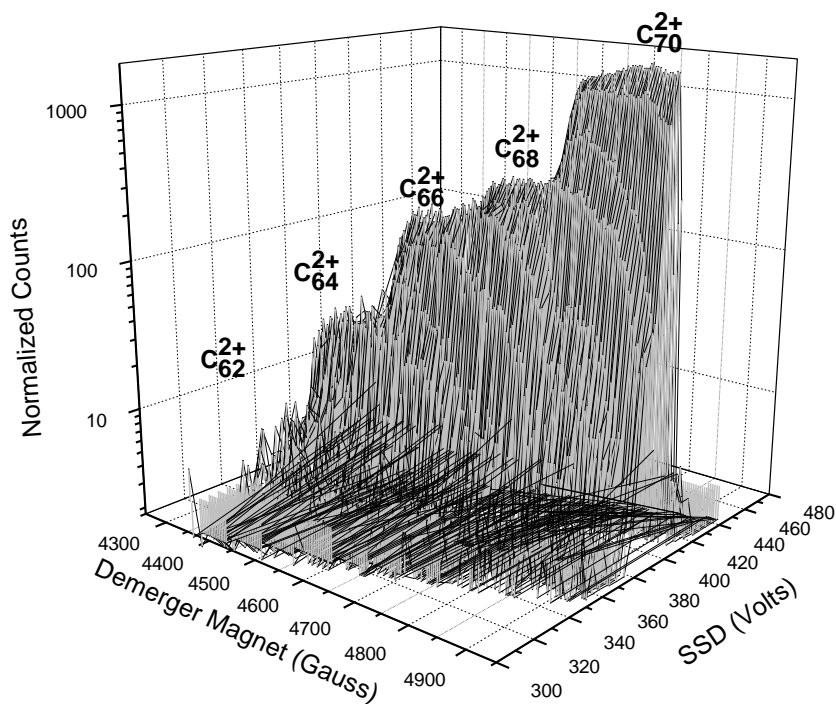


Figure 5.2 Two-dimensional photoionization/fragmentation scan of C_{70}^+ at 22eV

Another future experiment will be to obtain better statistics on the photoionization/fragmentation of $\text{Xe}@C_{60}^+$ in the photon energy region of the Xe 4d resonance. Kilcoyne *et al.* [33] have reported structure due to interference caused by reflection of the ejected photoelectron wave by the fullerene cage, termed confinement resonances.

Figure 5.3 compares the Xe 4d contribution to the spectrum of the photoionization/fragmentation of $\text{Xe}@C_{60}^+$ in the energy region of the Xe 4d resonance with different theoretical predictions. The powder prepared specifically for these experiments contains an extremely low fraction of the endohedral fullerenes, ($\sim 10^{-5}$), limiting ion beam currents to tens of fA and count rates to less than 0.5 Hz. Other techniques are being explored to trap more Xe atoms inside the fullerene cage and to purify the samples.

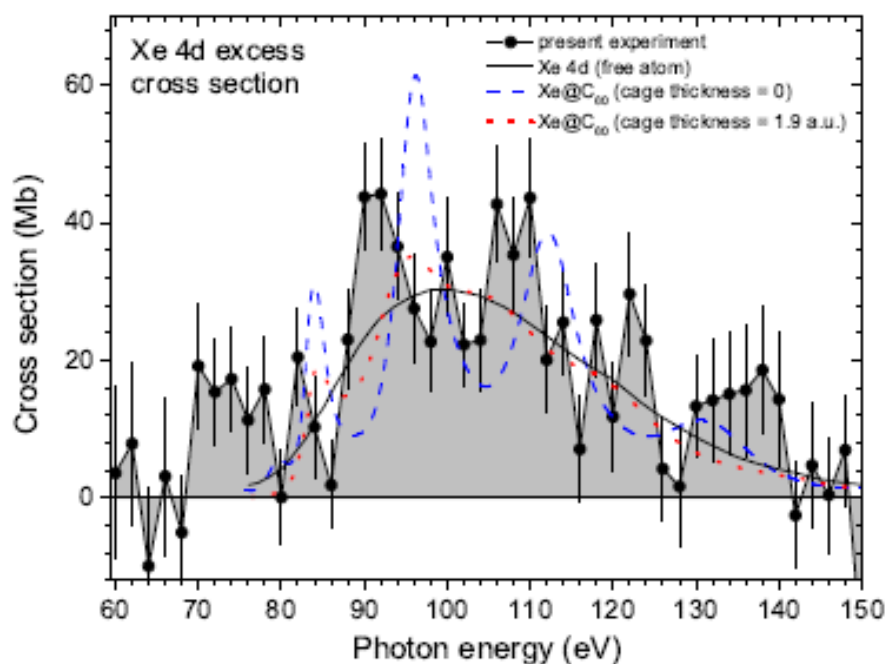


Figure 5.3 Excess Xe 4d cross section for double ionization with fragmentation of $\text{Xe}@C_{60}^+$ [33]

References

- [1] H. W. Kroto, J. R. Heath, S. C. O'Brien, R. F. Curl, and R. E. Smalley. C₆₀: Buckminsterfullerene. *Nature*, **318**:162, 1985.
- [2] Chemical of the Week. URL:
<http://scifun.chem.wisc.edu/chemweek/buckball/bucky.gif>
- [3] L. Becker, R. J. Poreda, A. G. Hunt, T. E. Bunch, and M. Rampino. Impact Event at the Permian-Triassic Boundary: Evidence from Extraterrestrial Noble Gases in Fullerenes. *Science*, **291**:1530, 2001.
- [4] D. A. García-Hernández, A. Manchado, P. García-Lario, L. Stanghellini, E. Villaver, R. A. Shaw, R. Szczerba, and J. V. Perea-Calderón. Formation of Fullerenes in H-Containing Planetary Nebulae. *Astrophys. J. Lett.*, **724**:L39, 2010.
- [5] I. V. Hertel, H. Steger, J. de Vries, B. Weisser, C. Menzel, B. Kamke, and W. Kamke. Giant Plasmon Excitation in Free C₆₀ and C₇₀ Molecules Studied by Photoionization. *Phys. Rev. Lett.*, **68**:784, 1992.
- [6] S. W. J. Scully, E. D. Emmons, M. F. Gharaibeh, R. A. Phaneuf, A. L. D. Kilcoyne, A. S. Schlachter, S. Schippers, A. Müller, H.S. Chakraborty, M. E. Madjet, and J. M. Rost. Photoexcitation of a Volume Plasmon in C₆₀ Ions. *Phys. Rev. Lett.*, **94**:065503, 2005.
- [7] C. Gause. Fullerene Nanomedicines for Medical and Healthcare Applications
<http://www.hhmglobal.com/knowledge-bank/articles/fullerene-nanomedicines-for-medical-and-healthcare-applications>

- [8] A. M. Covington, A. Aguilar, I. R. Covington, M. F. Gharaibeh, G. Hinojosa, C. A. Shirley, R. A. Phaneuf, I. Álvarez, C. Cisneros, I. Dominguez-Lopez, M. M. Sant'Anna, A. S. Schlachter, B. M. McLaughlin, and A. Dalgarno. Photoionization of Ne^+ using Synchrotron Radiation. *Phys Rev. A*, **66**:062710, 2002.
- [9] M. Habibi. Photoionization of the Cerium Isonuclear Sequence and Cerium Endohedral Fullerene. *Ph.D. Dissertation*, University of Nevada, Reno, 2009.
- [10] G. C. Baldwin and G. S. Kaliber. Photo-Fission in Heavy Elements. *Phys. Rev.*, **71**:3, 1947.
- [11] G. C. Baldwin and G. S. Kaliber. X-Ray Yield Curves for γ -n Reactions. *Phys Rev.*, **73**:1156, 1948.
- [12] M. Ya Amusia and J. P. Connerade. The Theory of Collective Motion Probed by Light. *Rep. Prog. Phys.*, **63**:41, 2000.
- [13] P. Andersen, T. Andersen, F. Folkmann, V. K. Ivanov, H. Kjeldsen, and J. B. West. Absolute Cross Sections for the Photoionization of 4d Electrons in Xe^+ and Xe^{2+} Ions. *J. Phys. B*, **34**:2009, 2001.
- [14] J. P. Connerade. A General Formula for the Profiles of 'Giant Resonances'. *J. Phys. B*, **17**:L165, 1984.
- [15] R. A. Phaneuf. "Plasmons in Fullerene Molecules." *Handbook of Nanophysics: Clusters and Fullerenes*. 'Ed'. K. D. Sattler. Boca Raton: CRC Press, 2011. Print.
- [16] R. D. Cowan. Atomic Theory of Atomic Structure and Spectra. *University of California Press*, Berkeley, 1981.

- [17] B. Konstant. Structure of the Truncated Icosahedron (Such as Fullerene or Viral Coatings) and a 60-Element Conjugacy Class in $PSI(2, 11)$. *Proc. Natl. Acad. Sci. USA*, **91**:11714, 1994.
- [18] H. Yang, B. Q. Mercado, H. Jin, Z. Wang, A. Jiang, Z. Liu, C. M. Beavers, M. M. Olmstead, and A. L. Balch. Fullerenes Without Symmetry: Crystallographic Characterization of $C_1(30)-C_{90}$ and $C_1(32)-C_{90}$. *Chem. Commun.*, **41**:2068, 2011.
- [19] C. Thilgen and F. Diederich. Structural Aspects of Fullerene Chemistry – A Journey through Fullerene Chirality. *Chem. Rev.*, **106**:5049, 2006.
- [20] J. B. West. Photoionization of Atomic Ions. *J. Phys. B* **34**:R45, 2001.
- [21] R. Trassl. Development of ECR Ion Sources. URL: http://www.strz.uni-giessen.de/~ezr/english/10ghz_perm.html, 2002.
- [22] René Bilodeau, Private Communication, 2010.
- [23] P. W. Fowler, D. E. Manolopoulos, G. Orlandi and F. Zerbetto. Energetics and Isomerisation Pathways of a Lower Fullerene: The Stone-Wales Map for C_{40} . *J. Chem. Soc. Faraday Trans.*, **91**:1421, 1995.
- [24] B. L. Henke, E. M. Gullikson, and J. C. Davis. X-Ray Interactions: Photoabsorption, Scattering, Transmission, and Reflection at $E = 50\text{--}30,000$ eV, $Z = 1\text{--}92$. *At. Data and Nucl. Data Tables* **54**:181, 1993.
- [25] W. Hofmann and G. L. Weissler. Measurement of the Photoionization Cross Section in the Resonance Continuum of C_I Using a Wall-Stabilized Arc. *J. Opt. Soc. Am.*, **61**:223, 1971.
- [26] X. Zhao. On the Structure and Relative Stability of C_{50} Fullerenes. *J. Phys. Chem. B*, **109**:5267, 2005.

- [27] J. Thomas, D. Bennett, and D. Puharic. The Fullerene Isomer Database. URL: <http://www.scribd.com/doc/36823152/The-Fullerene-Isomer-Database>, 2010.
- [28] S. J. Austin, P. W. Fowler, G. Orlandi, D. E. Manolopoulos, and F. Zerbetto. Relative Stabilities of C_{76} Isomers. A Numerical Test of the Fullerene Isolated-Pentagon Rule. *Chem. Phys. Lett.*, **226**:219, 1994.
- [29] A. V. Korol and A. V. Solov'yov. Comment of "Photoexcitation of a Volume Plasmon in C_{60} Ions". *Phys. Rev. Lett.*, **98**:179601, 2007.
- [30] M. Brack, P. Winkler, and M. V. N. Murthy. Coupling of Surface and Volume Oscillations in C_{60} Molecules. *Int. J. Modern Phys. E*, **17**:138, 2008.
- [31] Alfred Müller, Private Communication, 2011.
- [32] Bond Lengths and Energies. URL: <http://www.science.uwaterloo.ca/~cchieh/cact/c120/bondel.html>
- [33] A. L. D. Kilcoyne, A. Aguilar, A. Müller, S. Schippers, C. Cisneros, G. Alna'Washi, N. B. Aryal, K. K. Baral, D. A. Esteves, C. M. Thomas, and R. A. Phaneuf. Confinement Resonances in Photoionization of $Xe@C_{60}^+$. *Phys. Rev. Lett.*, **105**:213001, 2010.

Appendix

Tables of Absolute Photoionization Cross-Section Measurements

Table A.1 Absolute Photoionization Cross-Section Measurements for C_{40}^+

E(eV)	σ (Mb)	Uncertainty (Mb)
22	154	31
35	47.9	9.6
38	43.9	8.8
65	19.7	3.9

Table A.2 Absolute Photoionization Cross-Section Measurements for C_{50}^+

E(eV)	σ (Mb)	Uncertainty (Mb)
22	299	60
35	88.4	17.7
38	82.1	16.4
65	29.2	5.8

Table A.3 Absolute Photoionization Cross-Section Measurements for C_{60}^+

E(eV)	σ (Mb)	Uncertainty (Mb)
22	377	75
35	177	35
38	146	29
65	50.0	10.0

Table A.4 Absolute Photoionization Cross-Section Measurements for C_{70}^+

E(eV)	σ (Mb)	Uncertainty (Mb)
22	506	101
35	226	45
38	146	29
65	58.8	11.8

Table A.5 Absolute Photoionization Cross-Section Measurements for C_{76}^+

E(eV)	σ (Mb)	Uncertainty (Mb)
22	503	101
35	254	51
38	246	49
65	59.4	11.9

Table A.6 Absolute Photoionization Cross-Section Measurements for C_{78}^+

E(eV)	σ (Mb)	Uncertainty (Mb)
22	477	95
35	244	49
38	232	46
65	86.4	17.3

Table A.7 Absolute Photoionization Cross-Section Measurements for C_{84}^+

E(eV)	σ (Mb)	Uncertainty(Mb)
22	545	109
35	298	60
38	265	53
65	104	21